LETTER

doi:10.1038/nature14650

# Lanosterol reverses protein aggregation in cataracts

Ling Zhao[1,2,3]*†, Xiang-Jun Chen[4]*, Jie Zhu[3,5]*, Yi-Bo Xi[4]*, Xu Yang[6]*, Li-Dan Hu[4]*, Hong Ouyang[2,3], Sherrina H. Patel[3], Xin Jin[6], Danni Lin[3], Frances Wu[3], Ken Flagg[3], Huimin Cai[1,7], Gen Li[1], Guiqun Cao[1], Ying Lin[2,3], Daniel Chen[3], Cindy Wen[3], Christopher Chung[3], Yandong Wang[2], Austin Qiu[3,8], Emily Yeh[3], Wenqiu Wang[3,9], Xun Hu[1], Seanna Grob[3], Ruben Abagyan[10], Zhiguang Su[1], Harry Christianto Tjondro[4], Xi-Juan Zhao[4], Hongrong Luo[3], Rui Hou[7], J. Jefferson P. Perry[11], Weiwei Gao[3,12], Igor Kozak[13], David Granet[3], Yingrui Li[6], Xiaodong Sun[9], Jun Wang[6], Liangfang Zhang[3,12], Yizhi Liu[2], Yong-Bin Yan[5] & Kang Zhang[1,2,3,12,14]

**The human lens is comprised largely of crystallin proteins assembled into a highly ordered, interactive macro-structure essential for lens transparency and refractive index. Any disruption of intra- or inter-protein interactions will alter this delicate structure, exposing hydrophobic surfaces, with consequent protein aggregation and cataract formation. Cataracts are the most common cause of blindness worldwide, affecting tens of millions of people[1], and currently the only treatment is surgical removal of cataractous lenses. The precise mechanisms by which lens proteins both prevent aggregation and maintain lens transparency are largely unknown. Lanosterol is an amphipathic molecule enriched in the lens. It is synthesized by lanosterol synthase (LSS) in a key cyclization reaction of a cholesterol synthesis pathway. Here we identify two distinct homozygous *LSS* missense mutations (W581R and G588S) in two families with extensive congenital cataracts. Both of these mutations affect highly conserved amino acid residues and impair key catalytic functions of LSS. Engineered expression of wild-type, but not mutant, *LSS* prevents intracellular protein aggregation of various cataract-causing mutant crystallins. Treatment by lanosterol, but not cholesterol, significantly decreased preformed protein aggregates both *in vitro* and in cell-transfection experiments. We further show that lanosterol treatment could reduce cataract severity and increase transparency in dissected rabbit cataractous lenses *in vitro* and cataract severity *in vivo* in dogs. Our study identifies lanosterol as a key molecule in the prevention of lens protein aggregation and points to a novel strategy for cataract prevention and treatment.**

Cataracts account for over half of all cases of blindness worldwide, with the only established treatment involving surgical removal of the opacified lens. In developed nations, cataract surgeries amount to a significant portion of healthcare costs owing to the sheer prevalence of the disease among ageing populations. In addition, there is major morbidity associated with cataracts in developing countries, where there is limited access to surgical care.

High concentrations of crystallin proteins in lens fibres contribute to lens transparency and refractive properties[2]. The crystallin superfamily is composed of α-, β- and γ-crystallins, which are some of the most highly concentrated intracellular proteins in the human body. Protein aggregation is the single most important factor in cataract formation[3]. Factors that lead to protein aggregation include mutations in crystallin proteins, which are known to cause congenital cataracts, or oxidative stress, which in turn contributes to age-related cataracts. However, the precise mechanisms by which lens proteins maintain transparency or cause opacification are not completely understood.

Lanosterol synthase (2,3-oxidosqualene-lanosterol cyclase, LSS; EC 5.4.99.7) is encoded by the *LSS* gene. The LSS protein catalyses the conversion of (*S*)-2,3-oxidosqualene to lanosterol, which is a key early rate-limiting step in the biosynthesis of cholesterol, steroid hormones, and vitamin D (ref. 4). LSS was found to be expressed in the lens[5]. It was previously reported that the specific combination of hypomorphic mutations on *LSS* and *FDFT1* (farnesyl diphosphate farnesyl transferase 1) could decrease cholesterol levels in the lens and result in cataracts in Shumiya cataract rats (SCR)[6]. Here we identify novel homozygous mutations in the *LSS* gene in two consanguineous families and investigate the ability of lanosterol to alleviate protein aggregation and cataract formation.

We identified three children with severe congenital cataract from a consanguineous family of Caucasian descent (Fig. 1a). We performed whole-exome sequencing to an average of no less than 55-fold depth coverage on the target region (Extended Data Table 1a) in order to identify the causal mutation. On average, ~60,800–80,800 SNPs were detected in each exome (Extended Data Table 1b). Using a consanguineous recessive model and filtering against common variants (minor allele frequency >0.5%) in public databases, including dbSNP and the 1000 Genomes Project, as well as mutation function predictions (predicted by SIFT[7], Polyphen2[8], Phylop[9] and Mutationtaster[10]), we narrowed down potential candidate gene variants and identified a variant (G588S) in *LSS* on chromosome 21 as the most likely candidate (Extended Data Table 1c). Three affected children were homozygous for the G→A transition (G588S) in *LSS*, (GRch37/hg19: chr21:47615645; NM_001001438.2:c.1762G > A, NM_001001438.1: p.G588S), while the unaffected father, mother and remaining child were heterozygous for the change (Fig. 1a, b). Whole-genome SNP genotyping identified three long continuous homozygous regions in this family by HomozygosityMapper[11] (chr2:q22.1–q24.1, chr2:q31.1–q32.1 and chr21:q22.3; Extended Data Fig. 1a and Extended Data Table 1d). The *LSS* gene was located in one of the homozygous regions on chromosome 21 (Extended Data Fig. 1b). Furthermore, we screened for mutations in the *LSS* gene in 154 families with congenital cataracts and identified another homozygous mutation, W581R (GRch37/hg19: chr21:47615666; NM_001001438.2:c.1741T > C, NM_001001438.1: p.W581R), in a second consanguineous family (Fig. 1a, b, c). These two mutations were absent in 11,000 control chromosomes.

The amino acid residues W581 and G588 in LSS are highly conserved (Fig. 2a). We performed computational modelling analysis to

[1]Molecular Medicine Research Center, State Key Laboratory of Biotherapy, West China Hospital, Sichuan University, Chengdu 610041, China. [2]State Key Laboratory of Ophthalmology, Zhongshan Ophthalmic Center, Sun Yat-sen University, Guangzhou 510060, China. [3]Department of Ophthalmology and Biomaterials and Tissue Engineering Center, Institute for Engineering in Medicine, University of California San Diego, La Jolla, California 92093, USA. [4]State Key Laboratory of Membrane Biology, School of Life Sciences, Tsinghua University, Beijing 100084, China. [5]Department of Ophthalmology, Xijing Hospital, Fourth Military Medical University, Xi'an 710032, China. [6]BGI-Shenzhen, Shenzhen 518083, China. [7]Guangzhou KangRui Biological Pharmaceutical Technology Company, Guangzhou 510005, China. [8]CapitalBio Genomics Co., Ltd., Dongguan 523808, China. [9]Department of Ophthalmology, Shanghai First People's Hospital, School of Medicine, Shanghai JiaoTong University, Shanghai 20080, China. [10]Skaggs School of Pharmacy and Pharmaceutical Sciences, University of California, San Diego, La Jolla, California 92093, USA. [11]Department of Biochemistry, University of California Riverside, Riverside, California 92521, USA. [12]Department of Nanoengineering, University of California, San Diego, La Jolla, California 92093, USA. [13]King Khaled Eye Specialist Hospital, Riyadh, Kingdom of Saudi Arabia. [14]Veterans Administration Healthcare System, San Diego, California 92093, USA. †Present address: Institute of Molecular Medicine, Peking University, Beijing 100871, China.
*These authors contributed equally to this work.

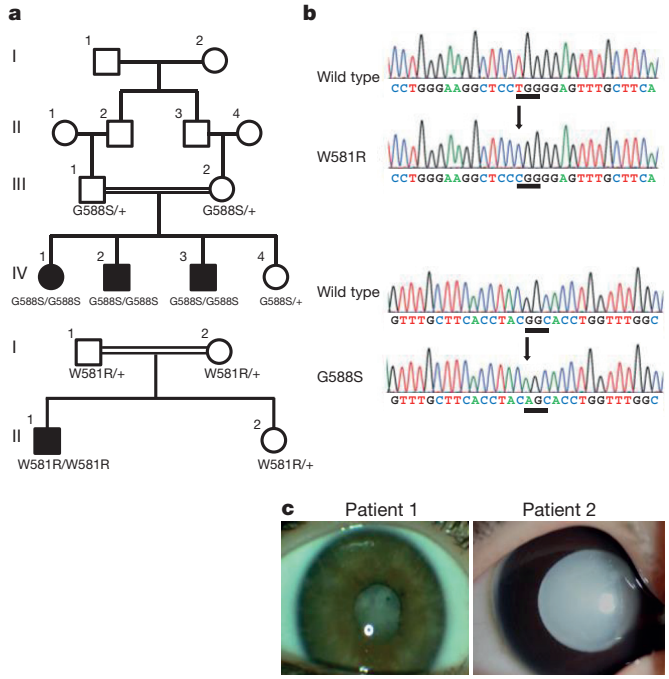


**Figure 1 | Identification of mutations in *LSS* causing congenital cataracts.** **a**, Pedigrees of affected families and cataract phenotype. Squares and circles indicate males and females respectively. +, wild-type allele; W581R and G588S are the two mutations. **b**, Upper panel, DNA sequencing data of an unaffected individual and an affected child (II-1) with a homozygous W581R mutation; lower panel, DNA sequencing data of an unaffected individual and an affected child (IV-1) with a homozygous G588S mutation. The underlined sequence indicates the nucleic acid change. **c**, Left, colour photograph of patient 1's right eye in the first pedigree (IV-1) with a total cataract; right, colour photograph of patient 2's right eye in the same pedigree (IV-3) with a cataract.

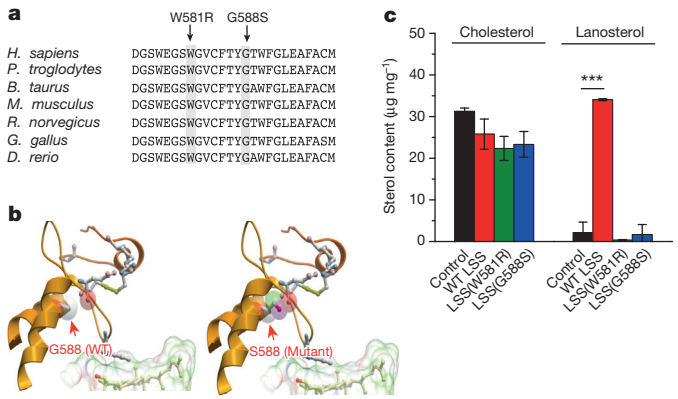


**Figure 2 | LSS mutations abolished the cyclase enzymatic function.** **a**, Conservation of W581R and G588 in LSS across several species: *Homo sapiens*, *Pan troglodytes*, *Bos taurus*, *Mus musculus*, *Rattus norvegicus*, *Gallus gallus* and *Danio rerio*. **b**, Computer modelling of LSS structure and impact of the LSS W581R and G588S mutations. A computer modelling analysis identifies a loop originating from C584 and ending at E578 with the key side chain of W581 at the tip of the loop stabilizing the sterol. The loop is fixed by an S–S bridge and the E578–R639 salt bridge. Amide nitrogen N of G588 interacts with the C584 from the previous helical turn and the Cα hydrogen of G588 is in close proximity to the critical E578, which then forms a strong salt bridge with R639 of the same supporting helix. The mutation G588S causes the side chain of the serine to clash into the E578 residue of the loop and is incompatible with the structure. Arrow indicates the location of the mutant side chain. **c**, Effect of engineered expression of the wild-type protein (WT LSS) and LSS mutants on sterol content. Wild-type LSS markedly increased lanosterol production, whereas neither W581R nor the G588S mutant exhibited any cyclase activity. $n = 3$ in each group; $^{***}P < 0.001$.

investigate the effects of the W581R and G588S mutations on the 3D structure and function of LSS. The amino acid tryptophan at position 581 has been reported to contribute to the catalytic site of the cyclase activity[12]. The G588S mutant was modelled by in-place replacement followed by side-chain refinement. The S588 side-chain refinement could not resolve the van der Waals clash between the serine side chain and the backbone carbonyl of E578, which forms a key salt bridge with R639. The orientation of the E579:C584 loop needed to be distorted to accommodate the mutation. The side chain of the mutant S588 clashed into an adjacent loop, indicating that the mutation was incompatible with the normal enzymatic structure and function of LSS (Fig. 2b). Supporting the *in silico* results, expression of wild-type LSS in a cell-transfection experiment exhibited cyclase activity and dramatically increased the amount of lanosterol production in the lipid fraction in HeLa cells, while neither the W581R nor the G588S mutant protein demonstrated any cyclase activity (Fig. 2c).

In contrast, the cholesterol level was unaffected by the expression of wild-type or mutant LSS, suggesting that there may be an alternative pathway for cholesterol homeostasis. The W581R and G588S mutations did not alter subcellular localization or cause aggregates of LSS protein when compared to that of wild-type LSS, suggesting that the cataract phenotype was not due to the formation of light-scattering particles by mutant LSS proteins themselves (Extended Data Fig. 2).

The aggregation of crystallins, the major structural proteins in the lens, is a predominant cause of various types of cataracts[3]. To mimic protein aggregation in the cataractous lens, six known cataract-causing mutant crystallin proteins were expressed in human lens progenitor cells, human lens epithelial line B-3 (HLEB-3), or HeLa cells. These mutant crystallins formed p62-positive inclusion bodies/aggresomes in all three transfected cell lines, suggesting that aggregation is an intrinsic property of mutant crystallins (Fig. 3a and Extended Data Figs 3 and 4)[13]. Co-expression of wild-type LSS and a cataract-causing mutant crystallin protein significantly reduced both the number and size of intracellular crystallin aggregates, whereas LSS mutants failed to do so alone (Fig. 3b, c and Extended Data Figs 3 and 4). Western blot analysis indicated that the Y118D mutant of αA-crystallin was released from intracellular aggregates and became more soluble with wild-type LSS (Fig. 3d and Extended Data Fig. 4c). Furthermore, addition of lanosterol, but not cholesterol, in the culture medium of cells co-expressing an LSS mutant and a mutant crystallin successfully reduced crystallin aggregation (Fig. 3c and Extended Data Figs 3 and 4). This result indicated that lanosterol, but not cholesterol, could be an effective agent to release mutant crystallin proteins from aggregation. Supporting this hypothesis, lanosterol significantly inhibited aggresome formation of both wild-type and mutated crystallin proteins in a concentration-dependent manner, while cholesterol had no effect (Fig. 3e, f and Extended Data Fig. 5). We further showed that lanosterol, but not cholesterol, increased the amounts of mutant crystallins in the soluble fractions of cell lysates (Fig. 3g and Extended Data Fig. 6a). Using serial live-cell imaging of cells expressing a GFP-fused Y118D mutant of αA-crystallin, we showed that addition of lanosterol could effectively diminish crystallin aggregates with a half-life of 222 ± 8 min (Fig. 3h), whereas addition of DMSO or cholesterol did not reduce aggresome formation (Extended Data Fig. 6b). Single-particle tracking in live cells clearly showed that lanosterol has an important role in the dissociation of pre-formed intracellular protein aggregates.

To investigate whether lanosterol has a direct effect on the dissolution of aggregated proteins, the aggregates of five wild-type and nine mutant crystallins were obtained by heating wild-type and mutated crystallins in the presence of 1 M guanidine chloride. Under this condition, all crystallin proteins formed amyloid-like fibrils as revealed by the enhancement of thioflavin T (ThT) fluorescence, the fibrillar structures under negatively stained transmission electron microscopy (TEM), and the low turbidity value (Fig. 4 and Extended Data Fig. 6c).

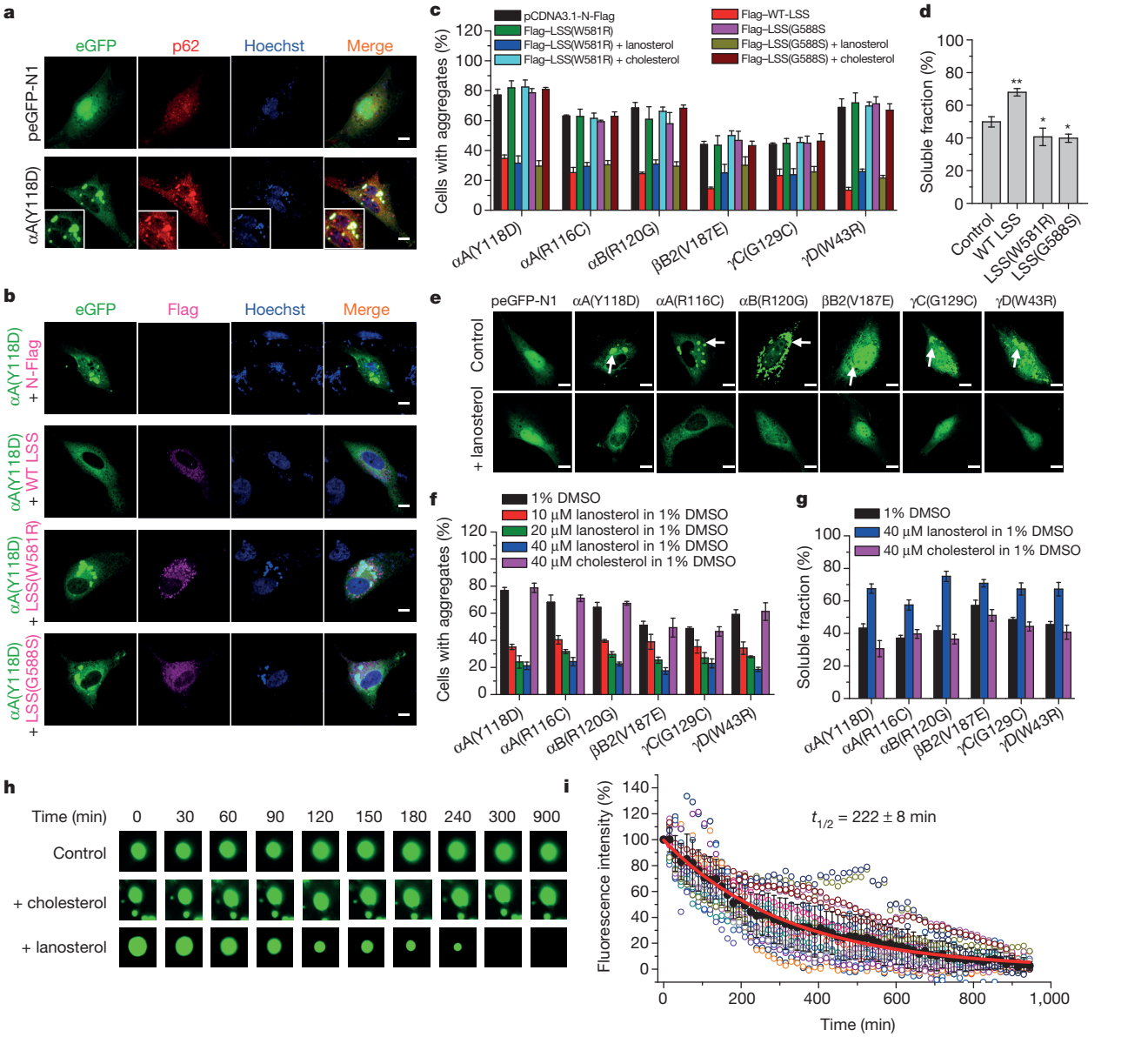


**Figure 3 | Lanosterol reduced intracellular aggregation of various crystallin mutant proteins.** **a**, Confocal images of crystallin protein aggregates in human lens progenitor cells. The cataract-causing Y118D mutant of αA-crystallin formed p62-positive intracellular inclusion bodies or aggresomes. Green, eGFP–crystallin proteins; red, p62; blue, nuclei. Cells transfected with peGFP-N1 were used as a control. **b**, Confocal images of the inhibitory effect of LSS on crystallin aggregates. **c**, Inhibition of crystallin mutant aggregation by wild-type LSS (WT LSS) and lanosterol, but not mutant LSS or cholesterol. **d**, Increase in soluble αA-crystallin(Y118D) mutant protein by co-expression of wild-type LSS but not LSS mutants (Y118D co-expressed with pcDNA3.1–N-Flag was used as a control). Quantitative analysis was performed using densitometry of crystallin proteins by western blot analysis of the supernatant or insoluble fraction of cell lysates. $n = 3$ in each group; representative western blot analysis is shown in Extended Data Fig. 4c; $^{*}P < 0.05$, $^{**}P < 0.01$. **e**, Confocal images of the re-dissolution of preformed crystallin aggregates by lanosterol. Arrows indicate the presence of crystallin aggregation. **f**, Lanosterol significantly reduced the intracellular aggregation by various cataract-causing mutant crystallin proteins in a concentration-dependent manner. $n = 3$; $P < 1 \times 10^{-4}$. Cholesterol did not reduce intracellular aggregation. $n = 3$; $P > 0.1$. **g**, Lanosterol increased the soluble fractions of various crystallin mutants in human lens progenitor cells. $n = 3$; $P < 0.001$. **h**, Effects of DMSO, cholesterol or lanosterol on αA-crystallin(Y118D) aggregates in human lens progenitor cells by serial live-cell imaging. Progression of crystallin aggregation dissolution by lanosterol can be observed, as evidenced by decreased green fluorescence following the time-course. **i**, Effect of lanosterol on dissolution of intracellular crystallin aggregates over time. $n = 22$ from three biological replicates. The 22 repetitions are shown in open circles distinguished by different colours. The mean ± s.d. values are shown as filled black circles and error bars. The data are best fitted by the single exponential decay process (red line). Scale bars, 10 μm.

The morphology of the amyloid-like fibrils obtained here was similar to those crystallin proteins reported previously[14]. We used PBS-containing liposomes formed by dipalmitoyl phosphatidylcholine (DPPC) to increase the solubility of sterol compounds and mimic the condition of sterols in cell membranes. Lanosterol, but not cholesterol, successfully re-dissolved the aggregated crystallin proteins from the amyloid-like fibrils in a concentration-dependent manner as indicated by the disappearance of fibrillar structures in the negatively stained TEM photographs and the decrease in ThT fluorescence intensity (Fig. 4 and Extended Data Fig. 6d). As an example, the re-dissolved αA-crystallins could be identified in negatively stained TEM pictures and were around 15 nm in size (Fig. 4a)[15].

To assess the effect of lanosterol on cataract reduction in lens tissues, we isolated naturally occurring cataractous lenses from rabbits. We incubated these cataractous lenses in a 25 mM lanosterol solution for 6 days and compared lens clarity before and after treatment of

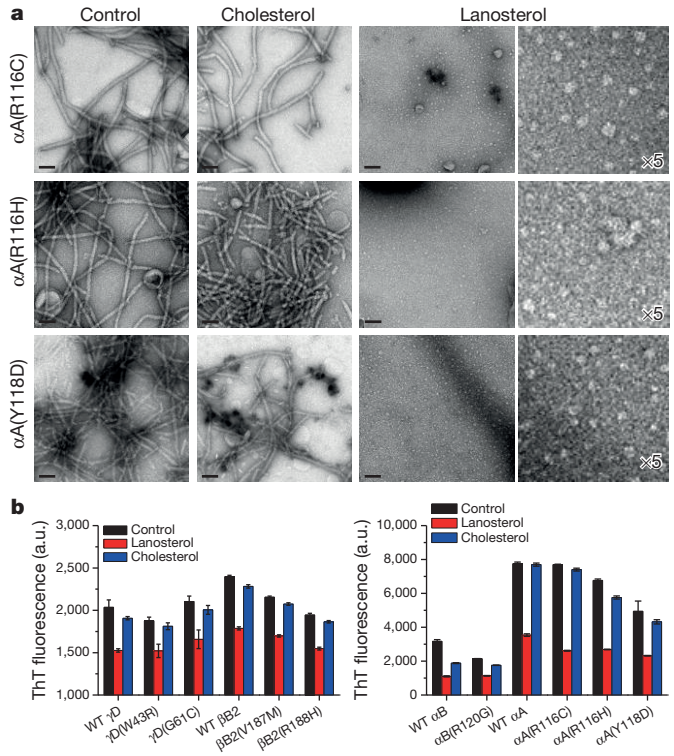


**Figure 4 | Lanosterol re-dissolved pre-formed amyloid-like fibrils of crystallin proteins.** **a**, Negatively stained TEM photographs of aggregates of αA-crystallin mutant proteins treated by a liposome vehicle, cholesterol or lanosterol in liposomes. Images in the right column of the lanosterol group show a 5× magnification of the image on their left. **b**, Effect of lanosterol on the re-dissolution of crystallin aggregates by ThT fluorescence ($n = 3$). Left, β/γ-crystallin mutants; right, α-crystallin mutants. Each bar results from three independent samples.

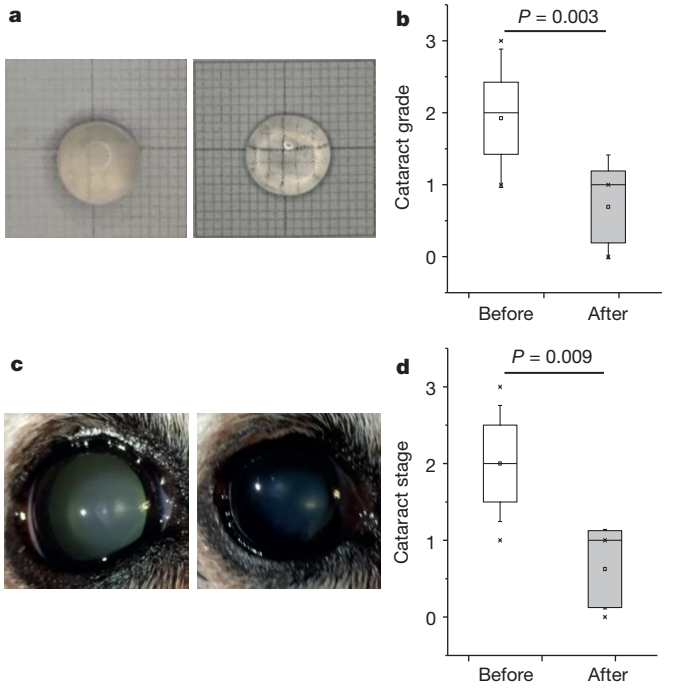


**Figure 5 | Lanosterol reduced cataract severity and increased clarity.** **a**, Photographs of a cataractous rabbit lens treated with lanosterol showing increased lens clarity. Left, before treatment; right, after. **b**, Boxplot of the quantification of the treatment effect of lanosterol ($n = 13$). **c**, Photographs of a cataractous dog lens treated with lanosterol showing increased lens clarity. Left, before treatment; right, after. **d**, Boxplot of the quantification of the treatment effect of lanosterol ($n = 7$). Range, median (horizontal line) and mean (circle) are presented. Crosses indicate the maximum and minimum cataract grades measured. Whiskers indicate the standard deviation and the box encompasses a 40% confidence interval.

lanosterol. We observed a strong trend of reduction in cataract severity, as demonstrated by an increase in lens clarity ($P < 0.003$, Wilcoxon Test, Fig. 5a, b, Extended Data Table 2a and Extended Data Fig. 7a, b). We further investigated the effect of lanosterol in reversing cataracts in dogs *in vivo*. Lanosterol treatment significantly reduced cataract severity and increased lens clarity ($P < 0.009$, Wilcoxon Test, Fig. 5c, d; Extended Data Table 2b and Extended Data Fig. 7c).

In this study, we demonstrated that homozygous mutations affecting the catalytic function of LSS cause extensive congenital cataracts with severe vision loss. The critical role of lanosterol in cataract prevention is supported by the observation that a rat strain harbouring compound *LSS* mutations recapitulates the human cataract disease phenotype[6]. Consistent with this notion, inhibition of LSS by U18666A, an LSS inhibitor (also known as an oxidosqualene cyclase inhibitor), was found to cause cataracts[16]. Furthermore, lanosterol treatment both decreased protein aggregation caused by mutant crystallin proteins in cell culture and reduced preformed cataract severity by increasing lens clarity in animal models. It is conceivable that the amphipathic nature of lanosterol allows it to intercalate into and coat hydrophobic core areas of large protein aggregates, effectively allowing these aggregations to gradually become water soluble again.

In summary, we show that lanosterol plays a key role in inhibiting lens protein aggregation and reducing cataract formation, suggesting a novel strategy for the prevention and treatment of cataracts. Cataracts are the leading cause of blindness and millions of patients every year undergo cataract surgery to remove the opacified lenses. The surgery, although very successful, is nonetheless associated with complications and morbidities. Therefore, pharmacological treatment to reverse cataracts could have large health and economic impacts. In addition, our results may have broader implications for the treatment of protein-aggregation diseases, including neurodegenerative diseases and diabetes, which collectively are a significant cause of morbidity and mortality in the elderly population, by encouraging the investigation of small-molecule approaches, such as the one demonstrated here.

**Online Content** Methods, along with any additional Extended Data display items and Source Data, are available in the online version of the paper; references unique to these sections appear only in the online paper.

**Received 7 July 2014; accepted 11 June 2015.**
**Published online 22 July 2015.**

1. Pascolini, D. & Mariotti, S. P. Global estimates of visual impairment: 2010. *Br. J. Ophthalmol.* **96,** 614–618 (2012).
2. Bloemendal, H. *et al.* Ageing and vision: structure, stability and function of lens crystallins. *Prog. Biophys. Mol. Biol.* **86,** 407–485 (2004).
3. Moreau, K. L. & King, J. A. Protein misfolding and aggregation in cataract disease and prospects for prevention. *Trends Mol. Med.* **18,** 273–282 (2012).
4. Huff, M. W. & Telford, D. E. Lord of the rings–the mechanism for oxidosqualene:lanosterol cyclase becomes crystal clear. *Trends Pharmacol. Sci.* **26,** 335–340 (2005).
5. Diehn, J. J., Diehn, M., Marmor, M. F. & Brown, P. O. Differential gene expression in anatomical compartments of the human eye. *Genome Biol.* **6,** R74 (2005).
6. Mori, M. *et al.* Lanosterol synthase mutations cause cholesterol deficiency-associated cataracts in the Shumiya cataract rat. *J. Clin. Invest.* **116,** 395–404 (2006).
7. Ng, P. C. & Henikoff, S. Predicting deleterious amino acid substitutions. *Genome Res.* **11,** 863–874 (2001).
8. Adzhubei, I. A. *et al.* A method and server for predicting damaging missense mutations. *Nature Methods* **7,** 248–249 (2010).
9. Pollard, K. S., Hubisz, M. J., Rosenbloom, K. R. & Siepel, A. Detection of nonneutral substitution rates on mammalian phylogenies. *Genome Res.* **20,** 110–121 (2010).
10. Schwarz, J. M., Cooper, D. N., Schuelke, M. & Seelow, D. MutationTaster2: mutation prediction for the deep-sequencing age. *Nature Methods* **11,** 361–362 (2014).
11. Seelow, D., Schuelke, M., Hildebrandt, F. & Nurnberg, P. HomozygosityMapper–an interactive approach to homozygosity mapping. *Nucleic Acids Res.* **37,** W593–W599 (2009).
12. Thoma, R. *et al.* Insight into steroid scaffold formation from the structure of human oxidosqualene cyclase. *Nature* **432,** 118–122 (2004).

13. Dobson, C. M. Protein folding and misfolding. *Nature* **426,** 884–890 (2003).
14. Ecroyd, H. & Carver, J. A. Crystallin proteins and amyloid fibrils. *Cell. Mol. Life Sci.* **66,** 62–81 (2009).
15. Braun, N. *et al.* Multiple molecular architectures of the eye lens chaperone αB-crystallin elucidated by a triple hybrid approach. *Proc. Natl Acad. Sci. USA* **108,** 20491–20496 (2011).
16. Cenedella, R. J. *et al.* Direct perturbation of lens membrane structure may contribute to cataracts caused by U18666A, an oxidosqualene cyclase inhibitor. *J. Lipid Res.* **45,** 1232–1241 (2004).

**Acknowledgements** We thank the study participants for their support. We thank G. Hannum, M. Kruppa, J. H. Shin, J. Mei, H. Zheng, F. Xu, J. Zhang, M. Kircher, J. Shendure, S. J. Fliesler, J. Gleeson, X.-T. Zuo, Y. Li and Y. Ding for their helpful advice during the course of the experiments and data analysis. This work is supported in part by grants from 973 Project (2015CB94600, 2012CB917304), 863 Program (2014AA021604), NSFC (31327901), State Key Laboratory of Ophthalmology, and State Key Laboratory of Membrane Biology.

**Author Contributions** L.Zhao, Y.Liu., Y.-B.Y., L.Zhang and K.Z. designed the study, interpreted data and wrote the manuscript. L.Z., X.-J.C., J.Z., Y.-B.X., X.Y., L.-D.H, H.O., S.H.P., X.J., D.L., F.W., K.F., H.C., G.L., G.C., Y.Li, D.C., C.W., C.C., Y.W., A.Q., E.Y., W.W., X.H., S.G., Z.S., H.C.T., X.-J.Z., H.L., R.H., J.J.P.P., W.G., I.K., D.G., and X.S. performed the experiments; R.A., Y.Li and J.W. contributed to data analysis and interpretation.

**Author Information** Reprints and permissions information is available at www.nature.com/reprints. The authors declare no competing financial interests. Readers are welcome to comment on the online version of the paper. Correspondence and requests for materials should be addressed to K.Z. (kang.zhang@gmail.com), Y.-B.Y. (ybyan@tsinghua.edu.cn), Y.Z.L. (yzliu62@yahoo.com) or L.Zhang (zhang@ucsd.edu).

## METHODS

**Study participants.** This study was approved by the Institutional Review Boards of Zhongshan Ophthalmic Center of Sun Yat-sen University, Sichuan University and the University of California, San Diego. Informed consent was obtained from all subjects before participation in the study. All participants underwent standard complete ophthalmic examinations and imaging studies. Demographic data, risk factors, and blood samples were collected at the initial visit. We recruited a consanguineous family consisting of two adults and four children. The parents were first cousins, and three of their four children were diagnosed with cataracts (Fig. 1a). We screened for *LSS* mutations in an additional 154 congenital cataract pedigrees and identified another family with a homozygous W581R mutation.

**Exome capture and sequencing.** Exome capture of phase I data (mother and three affected children) and phase II data (father and one unaffected daughter) were hybridized with NimbleGen 2.1M probe and Agilent SureSelect Human All Exon V2 according to the manufacturer's protocols, respectively. In brief, genomic DNA samples were randomly fragmented by Covaris with a base-pair peak of ~150–200 bp for the resulting fragments, and adapters were then ligated to both ends of the fragments. The adaptor-ligated templates were purified using Agencourt AMPure SPRI beads, and fragments with insert size ~250 bp were excised. Extracted DNA was amplified by ligation-mediated PCR, purified and hybridized to the SureSelect Biotinylated RNA Library (BAITS) for enrichment. Hybridized fragments bound to the strepavidin beads, whereas non-hybridized fragments were washed out after 24 h. Captured ligation-mediated PCR products were subjected to an Agilent 2100 Bioanalyzer to estimate the magnitude of enrichment. Each captured library was then loaded on Illunima Genome Analyzer II platform (phase I) or Hiseq 2000 (phase II), and paired-end sequencing was performed with read lengths of 90 bp, which provided at least 50× average coverage depth for each sample. Raw image files were processed by Illumina base-calling software for base calling with default parameters.

**Read mapping and variant detection.** Sequence reads in each individual were aligned to the human reference genome (NCBI build 37, hg19) using BWA[17](version 0.5.9–r16). BAM files created by BWA were then processed using the GATK[18] best practice pipeline using Genome Analysis ToolKit (version GATK 2.8) for re-alignment and variation (SNV and indel) detection. Variations that passed VQSR filtering criteria were extracted for the subsequent analyses.

**Candidate causal variant identification.** Variants were functionally annotated using ANNOVAR[19]. Missense, nonsense, and splicing mutations, which were likely to be deleterious when compared with synonymous and noncoding mutations, were extracted for analysis. Variants with a homozygous genotype in affected individuals and a heterozygous reference genotype in unaffected individuals, and a minor allele frequency <0.5% in both dbSNP137 and 1000 Genome Project databases (CEU) were considered as putative causal variants. Then, SIFT, Polyphen2, Phylop and Mutationtaster were used for function prediction, and mutations predicted to be damaging by no less than two tools were selected. Finally, variants that were shared as homozygous mutations within three affected children, as a heterozygous mutation in unaffected parents, and as heterozygous or homozygous to the reference genotype in unaffected daughter, but were absent in the public databases, were then considered as candidate causal variants.

**Whole-genome genotyping.** Whole-genome SNP genotyping was performed using Illumina HumanOmni 5Exome-4v1-1 array for all six family members. Mendelian error rate was calculated to check relative relationship in the family as part of quality control. Then, high-quality SNPs were selected for homozygosity mapping by HomozygosityMapper (http://www.homozygositymapper.org). HomozygosityMapper calculates the length of the homozygous block (in SNPs) at each marker for each sample. The values of the 'cases' are then added to get the 'homozygosity score' for a marker.

**Mutation screening of *LSS and FDFT1* genes.** Sanger DNA sequencing was performed to validate the G588S mutation in *LSS*. The 22 exons of the *LSS* gene were amplified by PCR and sequenced on the Genetic Analyzer 3130 (Applied Biosystems). The primers used to amplify the exons in *LSS* are presented in Extended Data Table 3a. We screened for mutations in the *LSS* gene in 154 families with congenital cataracts and identified another homozygous mutation, W581R, in a second consanguineous family. These two mutations were absent in 11,000 control chromosomes, including 2,000 chromosomes from an unaffected control population at the University of California, San Diego and the 1000 Genomes Project, and 8,000 chromosomes from an exome sequencing database at the University of Washington.

Due to a previous report that a *FDFT1* mutation modifies cataract phenotypes, we screened variants in the *FDFT1* gene, identifying only one common non-synonymous variant rs4731 (GRch37/hg19: chr8:11666337; NM_001287742.1: c.134A > G, NM_001274671.1:p.K45R). The variant was excluded as the causal mutation since an unaffected daughter harboured the same homozygous change, and a relatively high frequency of general population possess this variant (minor allele frequency >4% in 1000 Genome Project data) (Extended Data Table 1e).

**3D modelling of the G588S mutation.** The model of the G588S mutant was built from two structures as determined by Ruf *et al.*[20] and deposited in the Protein Data Bank as entries 1W6K and 1W6J[12]. The X-ray coordinates were used to build a full-atom model of the enzyme, and it was refined using the Internal Coordinate Mechanics program (ICM) and its PDB conversion protocol[21]. To analyse the effect of the G588S-mutation-induced clash on lanosterol binding, we analysed all side chains involved in the pocket of the enzyme interacting with lanosterol using the 1W6K structure. The areas of contact were calculated as the differences between the solvent-accessible area of each residue with and without lanosterol and were sorted by size using the ICM program[22].

**Plasmid constructs and site-directed mutagenesis.** The clone containing *LSS* cDNA was purchased from Thermo Scientific Inc. The coding sequence of wild-type LSS was cloned and inserted into the pcDNA3.1-N-Flag plasmid (Invitrogen). The mutants were constructed via site-directed mutagenesis by overlap extension using PCR. The common PCR primers were: NdeI forward, 5′-CATATGACGG AGGGCACGTGTCT-3′ and XhoI reverse, 5′-CTCGAGTCAGGGGTGGCCA GCAAG-3′. The primers for constructing the W581R and G588S mutants were: W581R forward, 5′-TGGGAAGGCTCCCGGGGAGTTTGCT-3′; reverse, 5′-GTGAAGCAAACTCCCCGGGAGCCTTC-3′; G588S forward, 5′-GCTTCACCTACAGCACCTGGTTTG-3′; G588S reverse, 5′-CCAAACC AGGTGCTGTAGGTGAAG-3′. The recombinant pcDNA3.1-N-Flag plasmids containing the wild-type or mutated *LSS* genes were transformed into *E. coli* DH5α cells. The cDNA of αA-, αB-, βB2-, γC- and γD-crystallin were cloned from the total cDNA of human lens as described previously[23–26]. The mutants were constructed by site-directed mutagenesis using the primers listed in Extended Data Table 3b. The amplified fragments were digested by XhoI and BamHI, and then inserted into the eukaryotic expression vector peGFP-N1 or the prokaryotic expression vector pET28a. The plasmids were obtained using the Plasmid Maxiprep kit (Vigorous) and verified by DNA sequencing. Crystallin gene constructs were made as a C-terminus eGFP fusion protein, while LSS was made as an N-terminal Flag-tagged protein.

**Cell culture and transfection.** HeLa cells and human lens epithelial B-3 cells (HLEB-3) were obtained from ATCC. Human lens progenitor cells were isolated from a fetal human eye[27]. The HeLa cells were cultured in DMEM medium containing 10% FBS (Gibco). The HLEB-3 cells were cultured in F12 medium with 20% FBS, while human lens progenitor cells were cultured in MEM medium containing 20% FBS and 10 μg ml$^{-1}$ FGF (Gibco). All cells were cultured at 37 °C in 5% $CO_2$ incubator. Cells routinely tested negative for mycoplasma contamination.

To assess the effect of *LSS* expression on sterol content, HeLa cells were transfected with wild-type *LSS* or *LSS* mutants fused with a Flag tag at the N-terminus of the coding region. The cells were harvested after 24 h transfection and the lipid fraction was extracted for LC–MS analysis. Cells transfected with the vector pcDNA3.1-N-Flag plasmids were used as a control. The expression levels of the wild-type and mutant LSS were normalized by western blot analysis using mouse anti-Flag (F1804; Sigma-Aldrich) and mouse anti-actin antibodies (BS6007M; Bioworld Technology).

To assess the effect of lanosterol on crystallin aggregation, human lens progenitor cells were co-transfected with *LSS* and various crystallin constructs for 4 h. Cells co-transfected with crystallin mutants and pcDNA3.1-N-Flag were used as a control. Human lens progenitor cells co-transfected with *LSS* and crystallin mutant constructs were cultured for 12 h before assaying for aggregates. The rescue experiments were performed after 16 h by addition of 40 μM sterols (lanosterol or cholesterol, Sigma-Aldrich) to the cell culture medium for 2 h, which was then replaced with fresh culture medium and cells cultured for 24 h. The percentage of cells with crystallin aggregates was calculated from ten randomly selected viewing fields. The values of the wild-type LSS group, mutant group, and mutant plus lanosterol group were calculated. Cells treated with 1% DMSO were used as the controls.

The impact of LSS and lanosterol on intracellular crystallin aggregation were evaluated in single-blinded observer studies. Experiments have been repeated at least three times. *P* values were calculated using Student's *t*-tests.

**Fluorescence microscopy.** Equal amounts of the human lens progenitor cells, HLEB-3 cells or HeLa cells were seeded on glass coverslips pretreated with TC (Solarbio). After culturing for 24 h to reach 90% confluency, the cells were transfected with plasmids containing various *LSS* or crystallin genes or co-transfected with plasmids containing a certain crystallin gene and those containing the wild-type or mutated *LSS* gene. The controls were cells transfected with the plasmids containing peGFP-N1 and/or peDNA3.1-N-Flag. Both transfection and co-transfection were performed using Lipofectamine 3000 (Invitrogen) according to the instructions from the manufacturer.

The effect of wild-type or mutated LSS on the intracellular aggregation of various cataract-causing crystallin mutants was evaluated by co-expression of

Flag–LSS and crystalline–GFP in the human lens progenitor cells, HLEB-3 cells or HeLa cells. The intracellular distributions of the proteins were visualized using GFP or antibody against Flag. After co-transfection for 4 h, the cells were cultured in fresh media for 24 h, and then analysed by microscopy.

The effect of lanosterol or cholesterol on the aggresome formation of various crystallins was studied by transfecting the cells with plasmids containing various crystallin genes. The cells were incubated for 24 h to enable efficient protein expression and aggresome formation. The cells were then treated with 0–40 μM sterols in 1% (for human lens progenitor cells) or 2% DMSO (for HeLa cells). Cells treated with 1% or 2% DMSO were used as the control. After treatment for 2 h, the media was replaced with fresh media. After 12 h, the cells were used for microscopy analysis.

The microscopy samples were prepared by washing the slips with phosphate buffered saline (PBS) three times. The cells were fixed with 4% paraformaldehyde for 40 min followed by another three washes with PBS. The cells were permeabilized with 0.1% Triton X-100 (Sigma) in PBS for 10 min and blocked with 5% normal goat serum in PBS for 1 h at 37 °C. Immunostaining was carried out by adding mouse anti-Flag antibody (1:500) or mouse anti-p62 antibody (1:200, ab56416; Abcam) in PBS buffer containing 5% normal goat serum and incubated for 1 h at 37 °C. Then the slips were washed three times with PBS, and further incubated with Alexa 649-conjugated goat anti-mouse IgG (1:250) for 1 h at ambient temperature. The nuclei were counterstained with Hoechst 33342 (Invitrogen). The mounted cells were analysed using a Carl Zeiss LSM 710 confocal microscope.

**Live-cell imaging.** Human lens progenitor cells were transfected with plasmids containing αA-crystallin(Y118D) mutant. After a 24 h transfection period, the cells with stable expression of αA-crystallin(Y118D) mutant were screen by incubation in culture medium containing 0.8 μg ml$^{-1}$ G418 for 7 days. Then the obtained cells were seeded onto glass bottom cell culture dishes (In Vitro Scientific) and treated with 1% DMSO, 40 μM cholesterol in 1% DMSO or 40 μM lanosterol in 1% DMSO for 4 h. Fresh culture medium was added, and the cells were analysed by serial live-cell imaging. Live-cell images were viewed with an Olympus IX81 microscope and captured with CellSens Dimension software (Olympus). Quantitative analysis of the size of aggregates was performed by measuring the fluorescence intensity of p62-positive aggregates using single-particle tracking in live-cell imaging. The live-cell imaging was conducted using three biological replicates with 1–8 repetitions each.

**Lipid extraction of the cells.** Extraction of lipids was performed using the Bligh and Dyer method[28]. In brief, ~$1 \times 10^6$–$10^7$ HeLa cells were washed 3–5 times with PBS and then scraped in 400-μl ice-cold methanol and transferred to a 1.5 ml Eppendorf tube with the addition of 200 μl chloroform. The samples were vortex-agitated for 1 min and then mixed with 300 μl of 1 M KCl. The organic and aqueous phases were separated by microcentrifugation at 20,817*g*. for 5 min at 4 °C. After separation, the lower organic phase was collected. Then the residual aqueous phase was re-extracted twice using 300 μl chloroform. The collected organic phases were dried using a SpeedVac sample concentrator under vacuum. The dried samples were stored at −80 °C for further LC–MS analysis.

**LC–MS analysis.** The dried lipid extracts were re-suspended in 100 μl methanol. The samples were vortex-agitated for 10 min, treated by 80 W ultrasonic sonication for 30 min, microcentrifuged at 20,817*g* for 10 min, and then the supernatant was transferred to a new Eppendorf tube. The microcentrifugation treatment was repeated three times. The derived samples were analysed by an Agilent 1290/6460 triple quadrupole LC/MS using an alternative Atmospheric Pressure Chemical Ionisation (APCI) source. The lipids were separated using an Agilent SB-C18 column. Selective ion monitoring was performed using the electron ionization mode. The highly pure lanosterol and cholesterol were used as controls. The MS determination was performed using a gas temperature of 350 °C, a gas flow rate of 4 l min$^{-1}$, a nebulizer of 60 p.s.i., a vaporizer of 350 °C, a capillary of 3,500 V and a corona current of 4 μA. To optimize the sensitivity and specificity, two qualifier ions were selected for the MS analysis of each compound (369.3/161.1 and 369.3/147 for cholesterol, and 409.2/191.3 and 409.2/109 for lanosterol).

**Western blotting.** The cell lysates were prepared in RIPA buffer containing 50 mM Tris (pH 8.0), 150 mM NaCl, 1% Triton X-100, 1 mM EDTA, 0.5% sodium deoxycholate and 0.1% SDS. The supernatant and precipitation fractions were separated by centrifugation. The proteins were separated by a 12.5% SDS–PAGE and transferred to a PVDF membrane (GE Healthcare). The mouse antibodies against Flag (F1804; Sigma-Aldrich) or GFP (MB2005; Bioworld Technology) were used to identify the overexpressed LSS and crystallin proteins, respectively. Quantification of the western blot bands was achieved using the software GELPRO (Media Cybernetics). The presented quantitative data were calculated from three independent experiments.

**Protein expression and purification.** The recombinant His-tagged wild-type and mutated β- and γ-crystallin proteins were overexpressed in *Escherichia coli* Rosetta and purified using an Ni-NTA affinity column followed by gel filtration chromatography using the same protocol as described elsewhere[23,24,26,29]. The overexpression and purification of the non-tagged αA- and αB-crystallins were performed as described previously[30]. The purity of the proteins was estimated to be above 95% as evaluated by one homogeneous band on 12.5% SDS–PAGE, 10% native-PAGE and a single peak in the size-exclusion chromatography profile. The protein concentration was determined according to the Bradford method by using BSA as the standard[31]. All protein samples were prepared in 20 mM PBS buffer containing 150 mM NaCl, 1 mM EDTA and 1 mM DTT.

**Protein aggregation and aggregate dissociation.** The aggregates of the wild-type and mutated αA- and αB-crystallin proteins were obtained by heating the protein solutions containing 1 M guanidine chloride (ultrapure, Sigma-Aldrich) at a concentration of 5 mg ml$^{-1}$ at 60 °C for 2 h. The aggregates of the wild-type and mutated β- and γ-crystallins were prepared by heating the protein solutions containing 1 M guanidine chloride at 37 °C for 48 h. The formation of aggregates was confirmed by ThT fluorescence, turbidity (absorbance at 400 nm) and transmission electron microscopy (TEM) observations. The preformed aggregates were re-suspended in 20 mM PBS with a final concentration of 0.2 mg ml$^{-1}$ (approximately 10 μM). The re-suspended aggregates were treated with 500 μM lanosterol or cholesterol in liposomes formed by 500 μM DPPC (Sigma-Aldrich) at 37 °C. Aggregates treated by 500 μM DPPC liposome were used as a negative control. After 24 h of treatment, the protein solutions were used for ThT fluorescence, turbidity and negatively stained TEM observations. The TEM samples were prepared by depositing the protein solutions onto a freshly glow-discharged carbon-coated copper grid. Negative-staining samples were obtained by staining the grid with 1.25% uranyl acetate for 30 s. The negatively stained TEM pictures were obtained on a Hitachi H-7650B transmission electron microscope with a voltage of 120 kV and a magnification of 48,000.

**Treatment of cataractous rabbit lenses.** This study was approved by IACUC of Zhongshan Ophthalmic Center and West China Hospital. Rabbits were euthanized by $CO_2$ inhalation and lenses were immediately dissected and treated with vehicle or lanosterol dissolved in vehicle to make 25 mM solutions. Lens tissues were incubated in these solutions for 6 days in the dark at room temperature. Cataracts were examined under a microscope and photographed. Degree of cataract was assessed by a blinded examiner using a previously described opacification grading system, shown below[32,33]. Improvements in lens clarity and transparency were quantified by visual inspection and grading. Lens clarity was scored by transmission of light, clarity of a grid image underneath the lense (Extended Data Fig. 7), and improvement in overall clarity of a lens or improvement in clarity of localized areas of cortical cataract. Wilcoxon test was used to evaluate the treatment effect.

**Cataract grading system.**

- Grade 0: absence of opacification (gridlines clearly visible);
- Grade 1: a slight degree of opacification (minimal clouding of gridlines, with gridlines still visible);
- Grade 2: presence of diffuse opacification involving almost the entire lens (moderate clouding of gridlines, with main gridlines visible);
- Grade 3: presence of extensive, thick opacification involving the entire lens (total clouding of gridlines, with gridlines not seen at all)

**Preparation of drug-loaded nanoparticles.** Lanosterol was loaded into a lipid-polymer hybrid nanoparticle through an adapted nanoprecipitation method[34]. In brief, the desired concentration of lanosterol was mixed with polycaprolactone (PCL) polymer dissolved in acetonitrile. Lecithin and 1,2-distearoyl-*sn*-glycero-3-phosphoethanolamine-*N*-carboxy(polyethylene glycol) 2000 (DSPE-PEG-COOH) were dissolved in a 4% ethanol aqueous solution at 20% of the PCL polymer weight and heated above 60 °C. The lanosterol/PCL solution was then added into the preheated lipid solution under gentle stirring followed by rigorous vortexing for 3 min. The mixture solution was then stirred for 2 h to allow the nanoparticles to form and the acetonitrile to evaporate. Next, the nanoparticle solution was washed three times using an Amicon Ultra-4 centrifugal filter (Millipore) with a molecular weight cut-off of 10 kDa to remove the remaining organic solvent and free molecules. The resulting nanoparticles were then re-suspended in PBS buffer for subsequent use. The size, size distribution, and surface zeta potential of the drug-loaded nanoparticles were characterized by dynamic light scattering. The loading yield of lanosterol was quantified by high-performance liquid chromatography.

**Treatment of cataractous lenses in dogs.** This study was approved by IACUC of Zhongshan Ophthalmic Center and West China Hospital. The following adult dog breeds were used for assessing the treatment effect: black Labrador, Queensland Heeler, Miniature Pinscher. All dogs were adult, non-diabetic and had normal ocular surfaces and ocular adnexa, with naturally occurring adult onset cataracts. There were near equal distributions of male and female dogs. We screened all exons of the *LSS* gene in these dogs and did not find any mutations. To assess the effect of lanosterol treatment on cataracts in live animals, dogs were pre-medicated

with intramuscular injections of acepromaxine and butorphanol. After 20 min, induction of anaesthesia was performed by application of intravenous propofol. Dogs were then immediately intubated and maintained on oxygen and 2% isoflurane at 2 l $min^{-1}$. Lanosterol (100 μg)-loaded nanoparticles were initially injected into the vitreous cavity in the test eye using a 28-gauge needle, and then were given every 3 days for the duration of the experiment. Treatment eyes or sham eyes were randomized. The control eye was given an injection with empty nanoparticle carriers as a negative control. The treatment eyes were treated with lanosterol in topical eye drops (see below for eye drop formulation). One 50-μl drop of lanosterol was administered three times daily to the test eye over 6 weeks. Degree of cataract severity was examined by slit lamp and photographed at the beginning and the end of the 6-week treatment period. Prior to examinations, pupils were dilated with 1% tropicamide and 10% phenylephrine. Degree of cataract severity was assessed by a blinded examiner and scored based on canine cataract stage, shown below[35]. Improvements in lens clarity and transparency were quantified. Wilcoxon test was used to evaluate the treatment effect.

**Grading system of canine cataracts.**

- Grade 0: absence of opacification (no cataract);
- Grade 1: a slight degree of opacification (incipient stage);
- Grade 2: presence of diffuse opacification involving almost the entire lens (immature stage);
- Grade 3: presence of extensive, thick opacification involving the entire lens (mature stage)

**Topical vehicle solution.** Double distilled $H_2O$ was added to 1.1 g $(EDTA)_2Na$ combined with 0.055 g alkyldimethylbenzylammonium chloride until a final volume of 1.1 l (pH 5.66) was achieved.

**25 mM lanosterol in the topical vehicle solution.** Double distilled $H_2O$ was added to a mixture of 12.5 g lanosterol, 1.1 g $(EDTA)_2Na$, 0.055 g alkyldimethylbenzylammonium chloride and 200 ml EtOH to a final volume of 1.1 l.


17. Li, H. & Durbin, R. Fast and accurate long-read alignment with Burrows–Wheeler transform. *Bioinformatics* **26,** 589–595 (2010).
18. DePristo, M. A. *et al.* A framework for variation discovery and genotyping using next-generation DNA sequencing data. *Nature Genet.* **43,** 491–498 (2011).
19. Wang, K., Li, M. & Hakonarson, H. ANNOVAR: functional annotation of genetic variants from high-throughput sequencing data. *Nucleic Acids Res.* **38,** e164 (2010).
20. Ruf, A. *et al.* The monotopic membrane protein human oxidosqualene cyclase is active as monomer. *Biochem. Biophys. Res. Commun.* **315,** 247–254 (2004).
21. Cardozo, T., Totrov, M. & Abagyan, R. Homology modeling by the ICM method. *Proteins* **23,** 403–414 (1995).
22. Abagyan, R. & Argos, P. Optimal protocol and trajectory visualization for conformational searches of peptides and proteins. *J. Mol. Biol.* **225,** 519–532 (1992).
23. Xu, J. *et al.* The congenital cataract-linked A2V mutation impairs tetramer formation and promotes aggregation of βB2-crystallin. *PLoS ONE* **7,** e51200 (2012).
24. Wang, B. *et al.* A novel *CRYGD* mutation (p.Trp43Arg) causing autosomal dominant congenital cataract in a Chinese family. *Hum. Mutat.* **32,** E1939–E1947 (2011).
25. Gu, F. *et al.* A novel mutation in *AlphaA-crystallin (CRYAA)* caused autosomal dominant congenital cataract in a large Chinese family. *Hum. Mutat.* **29,** 769 (2008).
26. Li, X.-Q. *et al.* A novel mutation impairing the tertiary structure and stability of γC-crystallin (CRYGC) leads to cataract formation in humans and zebrafish lens. *Hum. Mutat.* **33,** 391–401 (2012).
27. Nagineni, C. N. & Bhat, S. P. Human fetal lens epithelial cells in culture: an in vitro model for the study of crystallin expression and lens differentiation. *Curr. Eye Res.* **8,** 285–291 (1989).
28. Bligh, E. G. & Dyer, W. J. A rapid method of total lipid extraction and purification. *Can. J. Biochem. Physiol.* **37,** 911–917 (1959).
29. Wang, S., Leng, X.-Y. & Yan, Y.-B. The benefits of being β-crystallin heteromers: βB1-crystallin protects βA3-crystallin against aggregation during co-refolding. *Biochemistry* **50,** 10451–10461 (2011).
30. Sun, T.-X., Das, B. K. & Liang, J. J. N. Conformational and functional differences between recombinant human lens αA- and αB-crystallin. *J. Biol. Chem.* **272,** 6220–6225 (1997).
31. Bradford, M. M. A rapid and sensitive method for the quantitation of microgram quantities of protein utilizing the principle of protein-dye binding. *Anal. Biochem.* **72,** 248–254 (1976).
32. Geraldine, P. *et al.* Prevention of selenite-induced cataractogenesis by acetyl-L-carnitine: an experimental study. *Exp. Eye Res.* **83,** 1340–1349 (2006).
33. Makri, O. E., Ferlemi, A. V., Lamari, F. N. & Georgakopoulos, C. D. Saffron administration prevents selenite-induced cataractogenesis. *Mol. Vis.* **19,** 1188–1197 (2013).
34. Zhang, L. *et al.* Self-assembled lipid–polymer hybrid nanoparticles: a robust drug delivery platform. *ACS Nano* **2,** 1696–1702 (2008).
35. La Croix, N. Cataracts: When to refer. *Top. Companion Anim. Med.* **23,** 46–50 (2008).

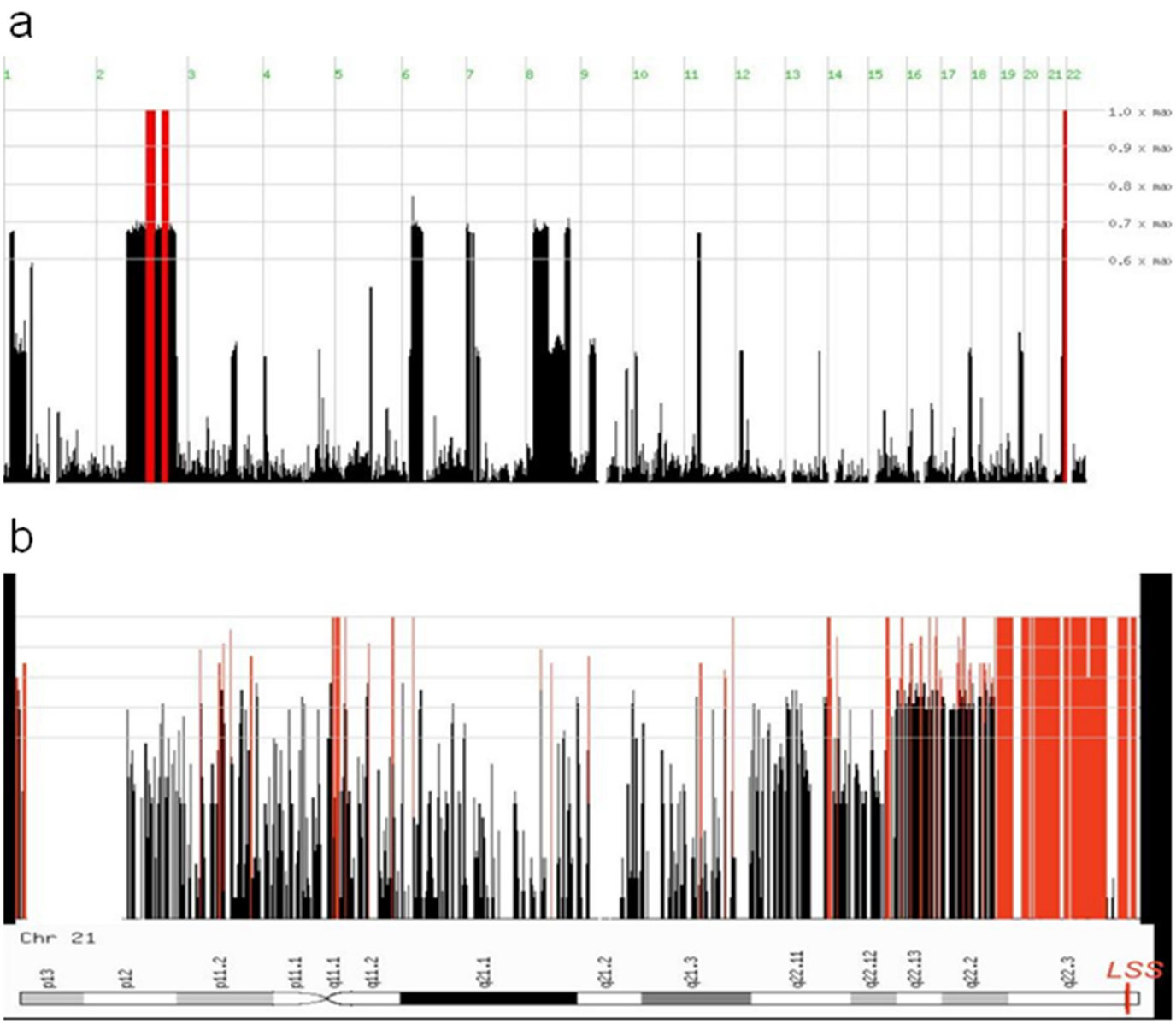


**Extended Data Figure 1 | Genome-wide homozygosity.** **a**, HomozygosityMapper plots the genome-wide homozygosity as bar charts. To emphasize regions of interest, any score higher than 80% of the maximum score reached in this project is coloured in red. **b**, The homozygosity scores were plotted against the physical position on chromosome 21, which contains the *LSS* gene. Red bars indicate regions with highest scores. The right side of the chromosome contains a long continuous homozygous region, where the *LSS* gene is located.

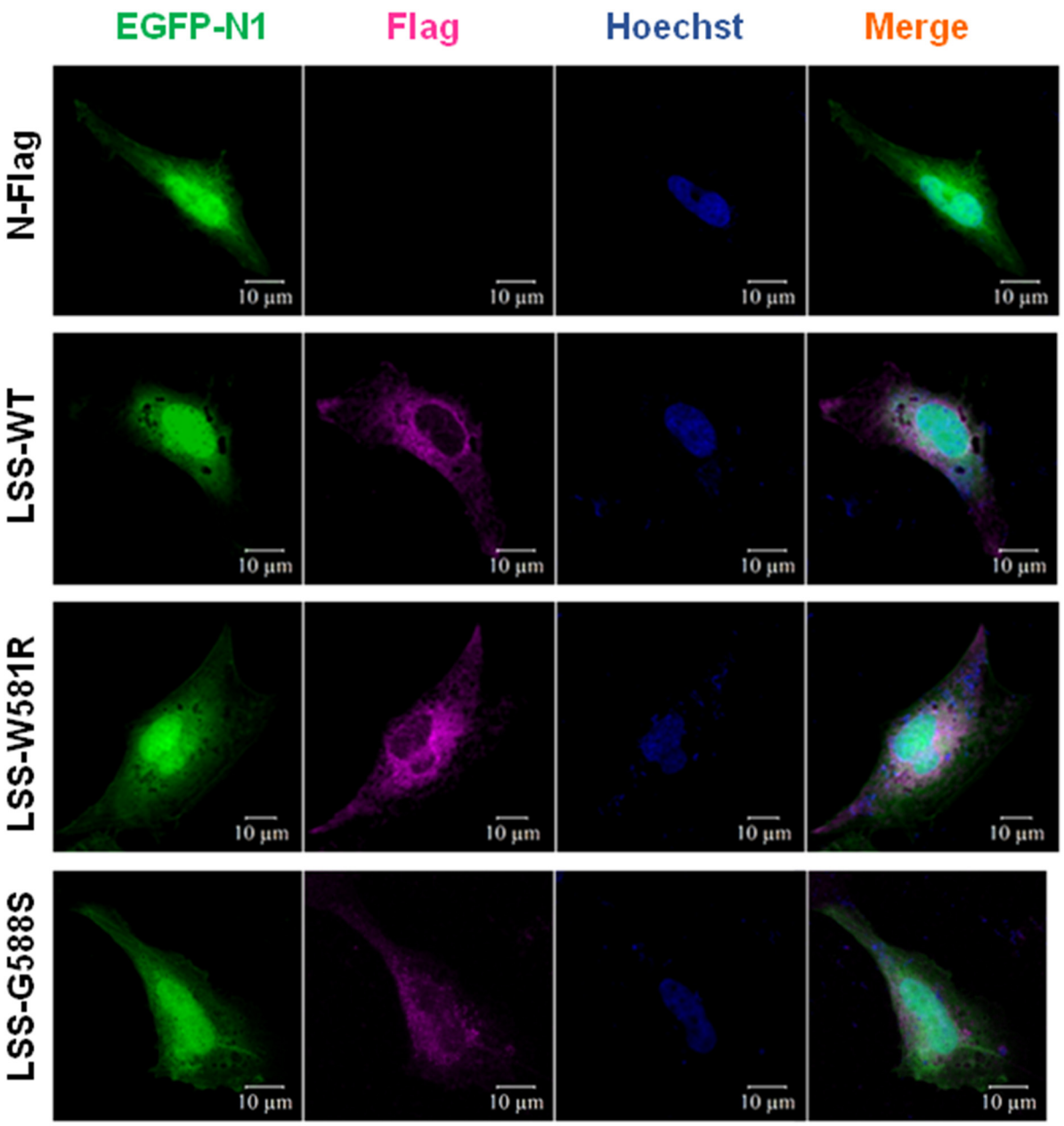


**Extended Data Figure 2 | Representative confocal images of cells co-transfected with Flag–LSS and eGFP.** Human lens progenitor cells were co-transfected with either the wild-type or the mutated *LSS* gene and the *eGFP* gene for 4 h and cultured for 16 h in fresh culture medium. The cellular distribution of LSS was then visualized using an anti-Flag antibody (purple). The distribution of eGFP (green) was used as a control. The nuclei were stained and visualized by Hoechst 33342 (blue).

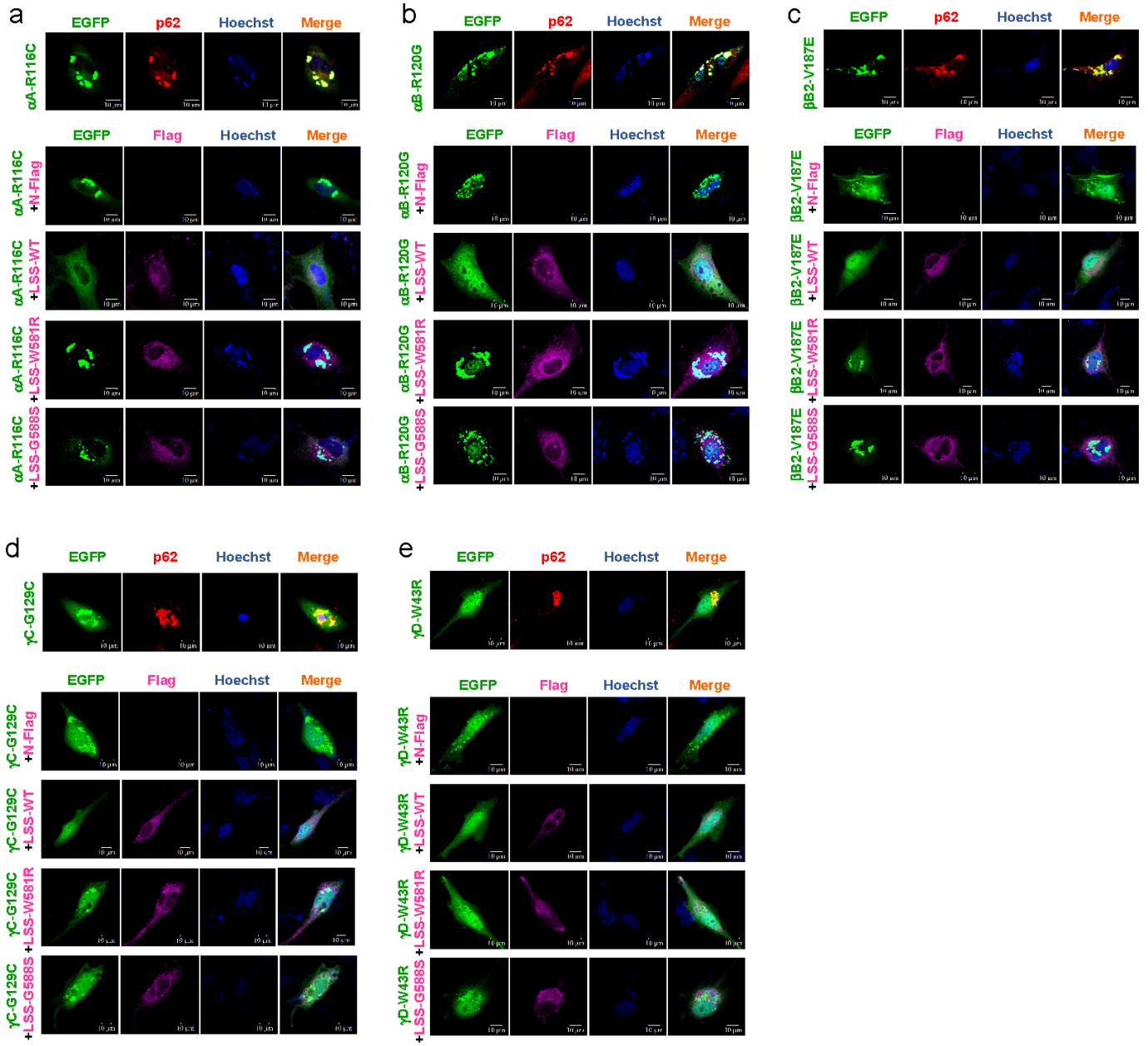


**Extended Data Figure 3 | Representative confocal images of cells co-transfected with LSS and various cataract-causing crystallin mutants.** **a**, R116C mutant of αA-crystallin. **b**, R120G mutant of αB-crystallin. **c**, V187E mutant of βB2-crystallin. **c**, G129C mutant of γC-crystallin. **e**, W43R mutant of γD-crystallin. Human lens progenitor cells were co-transfected with either the wild-type or the mutated Flag–LSS gene and the mutant GFP–crystallin gene for 4 h and cultured for 16 h in fresh culture medium. All crystallin mutants formed p62-positive aggregates as indicated by the co-localization of the mutant crystallins and p62. Cells co-transfected with GFP–crystallin and pcDNA3.1-N-Flag were used as controls. The formation of intracellular aggregates of various crystallin proteins was visualized by fluorescence of GFP (green). Wild-type or mutated LSS was detected with an anti-Flag antibody (purple), p62 was stained using an anti-p62 antibody (red), while the nuclei were stained and visualized by Hoechst 33342 staining (blue). Quantitative analysis of cells with aggregates is summarized in Fig. 3c.

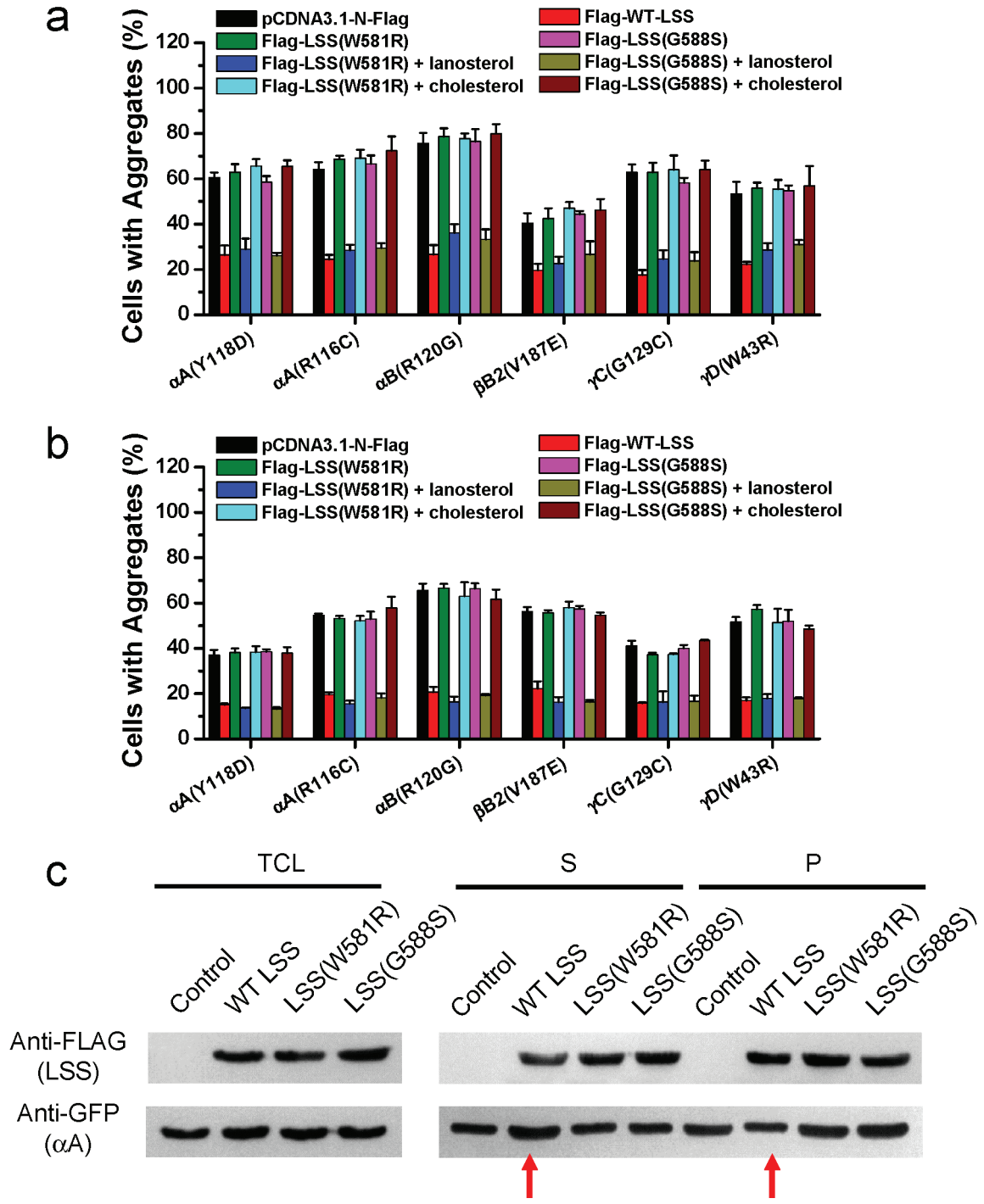


**Extended Data Figure 4 | Inhibition of crystallin mutant aggregation by wild-type LSS and lanosterol in HLEB-3 cells** (a) **or HeLa cells** (b)**.** Cells co-transfected with LSS and crystallin mutant constructs were cultured for 24 h before assaying for aggregates. The rescue experiments were performed by addition of 40 μM sterols (lanosterol or cholesterol) to the cell culture medium for 2 h, the sterol medium was then replaced with fresh culture medium and the cells were cultured for a further 12 h. The percentage of cells with crystallin aggregates were calculated from ten randomly selected viewing fields. The values of the wild-type LSS group, mutant group, or mutant plus lanosterol group were calculated. Aggregates were significantly lower in the wild-type LSS and lanosterol groups compared to the control group ($P < 1 \times 10^{-4}$), while aggregates in mutant LSS or cholesterol groups showed no difference to the control group ($P > 0.1$). **c**, Human lens progenitor cells were co-transfected with wild-type or mutant LSS plus αA-crystallin(Y118D). αA-crystallin(Y118D) co-expressed with pcDNA3.1-N-Flag was used as a control. After transfection for 4 h and incubation in fresh culture medium for another 24 h, the cells were lysed and centrifuged to separate supernatant and insoluble fractions. LSS and crystallin fusion proteins were detected by antibodies against Flag and GFP, respectively. Red arrows indicate higher crystalline content in the soluble fraction versus in the insoluble fraction in cells containing the WT-LSS. Data were quantified from three independent experiments and summarized in Fig. 3d.

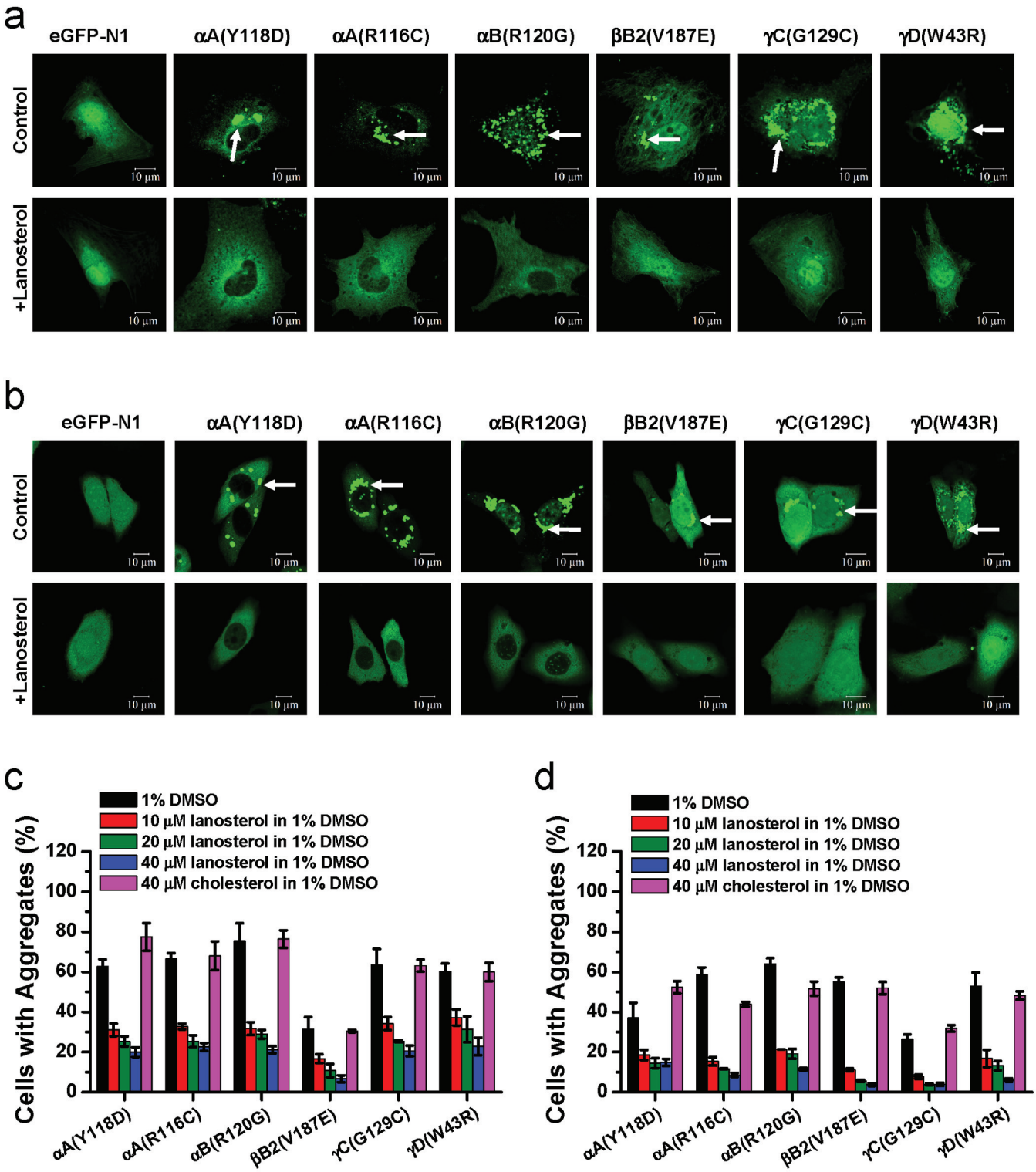


**Extended Data Figure 5 | Lanosterol significantly reduced the intracellular aggregation caused by various cataract-causing mutant crystallin proteins in a concentration-dependent manner when assayed in HLEB-3 or HeLa cells.** **a**, Representative confocal images of HLEB-3 cells transfected with various cataract-causing crystallin mutants. **b**, Representative confocal images of HeLa cells transfected with various cataract-causing crystallin mutants. Cells were transfected with various crystallin constructs for 4 h and cultured for an additional 24 h in fresh culture medium. Then the cells were treated with 10, 20 and 40 μM lanosterol in 1% (HLEB-3 cells) or 2% DMSO (HeLa cells) for 2 h and cultured for another 12 h. Cells treated with 1% (HLEB-3 cells) or 2% DMSO (HeLa cells) were used as the controls. Formation of intracellular aggregates of various crystallin proteins was visualized by fluorescence of GFP (green) and the nuclei were stained with Hoechst 33342 (blue). Typical intracellular aggregates are indicated by arrows. **c**, Concentration dependence of the aggregation-dissolving effects of lanosterol when assayed in HLEB-3 cells. **d**, Concentration dependence of the aggregation-dissolving effects of lanosterol when assayed in HeLa cells.

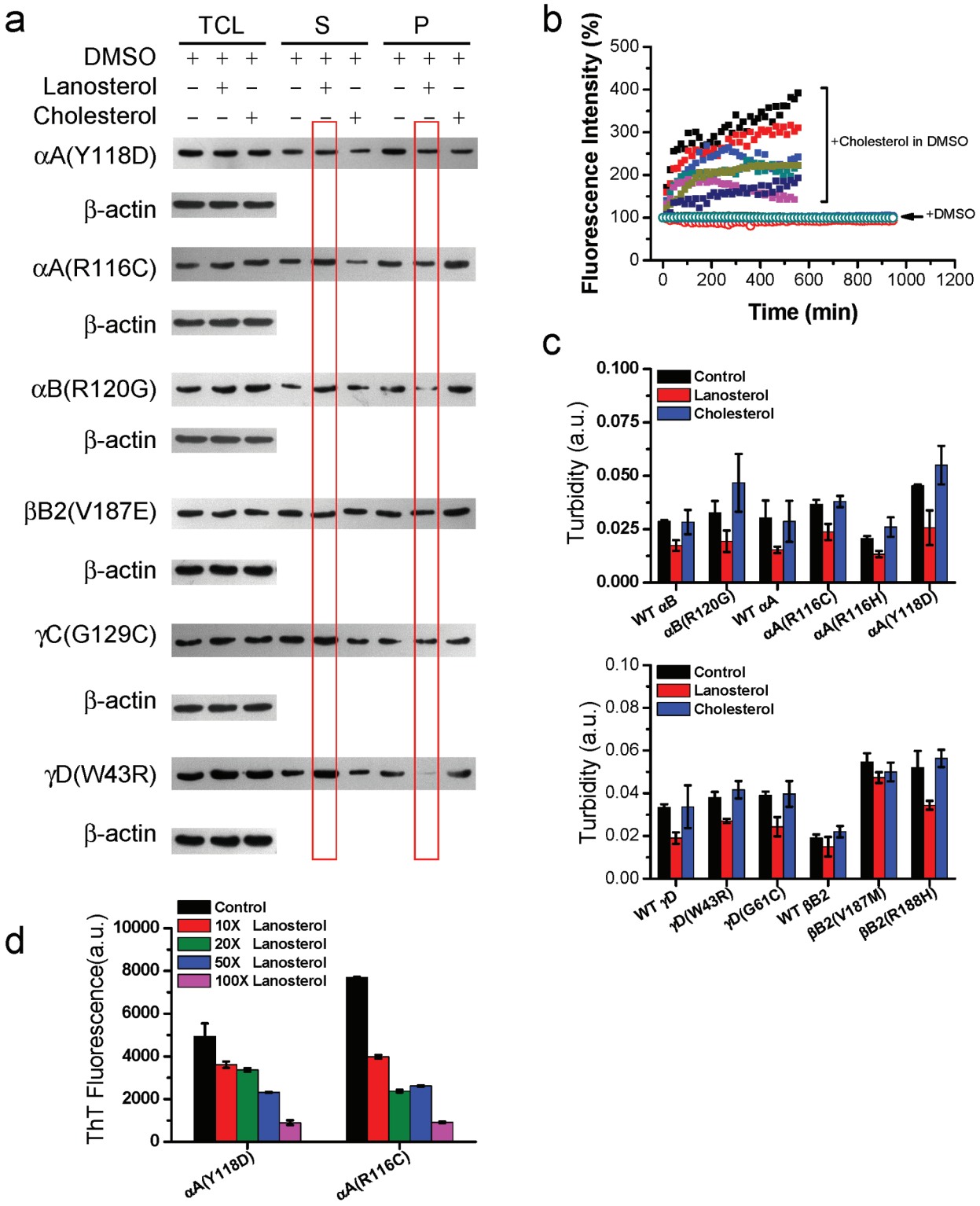


**Extended Data Figure 6 | Treatment by lanosterol, but not cholesterol, increased cataract-causing mutant crystallins in soluble fractions when compared to a control group or a mutant LSS group.** **a**, Human lens progenitor cells were transfected with mutant crystallin genes for 4 h, and then incubated in fresh culture medium for another 24 h. The cells were harvested and lysed. Supernatant and insoluble fractions were separated by centrifugation and analysed by western blot analysis. LSS and crystallin fusion proteins were identified by antibodies against Flag and GFP tags, respectively. The lanosterol-treated group is highlighted by red boxes. Cells treated with 1% DMSO were used as a control. β-Actin was used as an internal protein loading control of total cell lysates (TCL). S, supernatant; P, insoluble fraction. **b**, Effect of DMSO ($n = 4$) and cholesterol ($n = 7$) on the size changes of αA-crystallin(Y118D) aggregates in human lens progenitor cells evaluated by single-particle tracking in live-cell imaging. **c**, Evaluation of the effect of lanosterol on the dissolution of crystallin aggregates by turbidity. Crystallin aggregates were formed by incubating 5 mg ml$^{-1}$ protein solution at 60 °C for 2 h (α-crystallins) or 37 °C for 48 h (β- and γ-crystallins) in the presence of 1 M guanidine chloride. The preformed aggregates were re-suspended in PBS at a final protein concentration of 0.2 mg ml$^{-1}$ and were treated with 500 μM sterols in 500 μM DPPC liposome and incubated at 37 °C for 24 h. Aggregates treated with 500 μM DPPC liposome only were used as the controls. **d**, Concentration-dependent effect of lanosterol on the re-dissolution of amyloid-like fibrils by αA-crystallin mutants evaluated by ThT fluorescence. Aggregates treated with 500 μM DPPC liposome only were used as the controls.

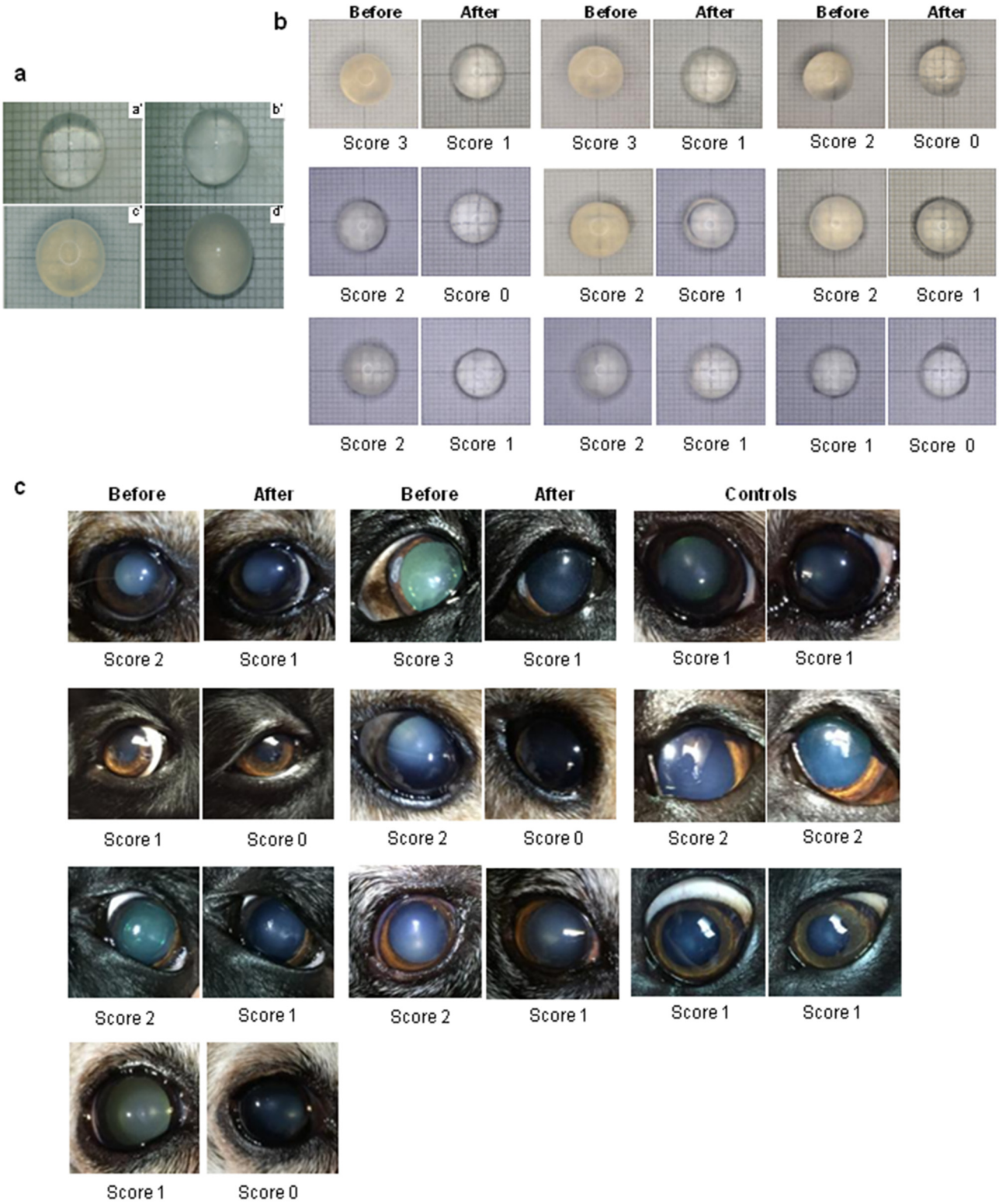


**Extended Data Figure 7 | Grading system of cataractous lenses.** **a**, Lenses were placed above a grid and photographed. The degree of transparency was scored as 0, a clear lens and absence of opacification (gridlines clearly visible, a′); 1, a blurry lens and a slight degree of opacification (minimal clouding of gridlines, with gridlines still visible, b′); 2, a cloudy lens and presence of diffuse opacification involving almost the entire lens (moderate clouding of gridlines, with main gridlines visible, c′); or 3, an opaque lens and presence of extensive thick opacification involving the entire lens (total clouding of gridlines, with gridlines not seen at all, d′). **b**, Lanosterol reduced cataract severity and increased clarity in isolated cataractous rabbit lenses. Rabbit lenses ($n = 13$) were dissected and incubated with lanosterol for 6 days and subsequently assessed for lens clarity and transparency. Pairs of photographs of each cataractous rabbit lens showing before and after treatment with scores underneath are shown. **c**, Lanosterol reduced cataract severity and increased lens clarity in dogs. Dog eyes with cataracts ($n = 7$) were treated with lanosterol for 6 weeks and assessed for lens clarity and transparency. A pair of photographs of each study eye before and after treatment is shown with scores underneath. Three control eyes treated with vehicles alone are also presented.

## Extended Data Table 1 | Exome sequencing and variants

**a**

| Sample | Total effective yield(Mb) | Average sequencing depth | Mismatch rate | Coverage of target region | Fraction of target covered >= 4x | Fraction of target covered >= 10x |
|---|---|---|---|---|---|---|
| IV-1 | 3,409.20 | 60.16 | 0.20% | 99.60% | 99.10% | 97.60% |
| IV-2 | 3,314.58 | 58.62 | 0.20% | 99.60% | 99.20% | 97.80% |
| IV-3 | 3,327.63 | 57.24 | 0.20% | 99.80% | 99.20% | 97.40% |
| III-2 | 3,029.40 | 51.89 | 0.21% | 99.80% | 99.30% | 97.70% |
| III-1 | 6,877.08 | 54.24 | 0.29% | 96.30% | 89.40% | 81.80% |
| IV-4 | 6,331.78 | 44.12 | 0.29% | 96.50% | 88.80% | 79.80% |

**b**

| Sample | Total variation | Heterzygotes | Homozygotes | missense | nonsense | readthrough | synonymous | splicing | intergenic | intronic |
|---|---|---|---|---|---|---|---|---|---|---|
| IV-1 | 61,189 | 35,571 | 25,618 | 6,105 | 69 | 39 | 7,296 | 32 | 5,371 | 36,598 |
| IV-2 | 60,829 | 34,698 | 26,131 | 6,074 | 62 | 41 | 7,211 | 38 | 5,178 | 36,572 |
| IV-3 | 61,078 | 35,238 | 25,840 | 6,221 | 78 | 43 | 7,265 | 38 | 5,099 | 36,544 |
| III-2 | 62,753 | 39,001 | 23,752 | 6,393 | 64 | 38 | 7,588 | 34 | 5,764 | 36,924 |
| III-1 | 80,067 | 49,694 | 30,373 | 7,247 | 93 | 49 | 8,166 | 47 | 15,063 | 41,391 |
| IV-4 | 80,893 | 48,211 | 32,682 | 7,252 | 85 | 50 | 8,184 | 50 | 14,547 | 42,414 |

**c**

| Filters | III-1 (carrier father) | III-2 (carrier mother) | IV-1 (affected daughter) | IV-2 (affected son) | IV-3 (affected son) | IV-4 (unaffected daughter) | Combine |
|---|---|---|---|---|---|---|---|
| Total variations | 80,067 | 62,753 | 61,189 | 60,829 | 61,078 | 80,893 | - |
| Missense, Nonsense, Splicing | 7,389 | 6,495 | 6,213 | 6,177 | 6,342 | 7,387 | - |
| Affected: 1/1; carrier: 0/1; unaffected: 0/1 or 0/0 * | 5,792 | 4,661 | 3,127 | 3,123 | 3,085 | 5,638 | 9 |
| Not in dbSNP | 3,724 | 2,969 | 1,954 | 1,929 | 1,928 | 3,589 | 5 |
| Not in 1000 Genomes Project | 1,032 | 767 | 227 | 264 | 245 | 1,059 | 1 |
| Predicted damaging | 267 | 269 | 31 | 45 | 41 | 264 | 1 |

*Homozygous in affected child, heterozygous in carrier, no homozygous mutants in unaffected child

**d**

| Sample | Total loci | Captured | SNP |
|---|---|---|---|
| IV-1 | 4,641,218 | 4,440,318 | 559,832 |
| IV-2 | 4,641,218 | 4,446,992 | 605,499 |
| IV-3 | 4,641,218 | 4,445,267 | 526,794 |
| III-2 | 4,641,218 | 4,448,054 | 537,925 |
| III-1 | 4,641,218 | 4,446,581 | 574,880 |
| IV-4 | 4,641,218 | 4,450,657 | 584,347 |

**e**

| Position (GRch37/hg19) | refSNP | REF | ALT | Function | III-1 (carrier father) | III-2 (carrier mother) | IV-1 (affected daughter) | IV-2 (affected son) | IV-3 (affected son) | IV-4 (unaffected daughter) |
|---|---|---|---|---|---|---|---|---|---|---|
| chr8:11666337 | rs4731 | A | G | nonsynonymous | A/G | A/G | G/G | A/G | G/G | G/G |
| chr8:11683653 | rs904011 | T | C | synonymous | C/C | C/C | C/C | C/C | C/C | C/C |

**a**, Summary of exome sequencing data production. **b**, Summary of detected variants. **c**, Variants prioritization pipeline after exome sequencing. **d**, Summary of whole-genome genotyping data. **e**, Coding variants detected on gene *FDFT1*.

**Extended Data Table 2 | Treatment effect of lanosterol in cataractous rabbit lenses and dog cataracts.**

**a**

| Sample number | Before treatment | After treatment |
|---|---|---|
| 1 | 3 | 1 |
| 2 | 2 | 0 |
| 3 | 2 | 1 |
| 4 | 2 | 0 |
| 5 | 3 | 1 |
| 6 | 2 | 1 |
| 7 | 2 | 1 |
| 8 | 2 | 0 |
| 9 | 1 | 1 |
| 10 | 1 | 0 |
| 11 | 2 | 1 |
| 12 | 1 | 1 |
| 13 | 2 | 1 |

Grading of the cataract severity was conducted by an examiner, blinded regarding the treatment status, based on a scale 0 to 3, as described in the Methods section.

**b**

| Study eye | Treatment group | | Control group | |
|---|---|---|---|---|
| | Before | After | Before | After |
| 1 | 2 | 1 | 1 | 1 |
| 2 | 1 | 0 | 2 | 2 |
| 3 | 2 | 1 | 1 | 1 |
| 4 | 3 | 1 | | |
| 5 | 1 | 0 | | |
| 6 | 2 | 0 | | |
| 7 | 2 | 1 | | |

Grading of the cataract formation was conducted by an examiner, blinded regarding the treatment status, based on a scale 0 to 3. 0 = no cataract, 1 = incipient, 2 = immature, and 3 = mature.

**a**, Treatment effect of lanosterol in cataractous rabbit lenses. Grading of the cataract severity was conducted by an examiner, blinded to treatment status, on a scale from 0 to 3, as described in the Methods. **b**, Treatment effect of lanosterol in cataractous dog lenses. Grading of the cataract formation was conducted by an examiner, blinded to treatment status, on a scale from 0 to 3. 0 = no cataract, 1 = incipient, 2 = immature, and 3 = mature.

**Extended Data Table 3 | Primers used for sequencing of each exon in the human *LSS* gene and construction of crystallin mutants**

**a**

| Amplicon | Sequence (5'-3') |
|---|---|
| LSS-Exon1-F | GCCTGAGCGCCTGCCGAGGCCT |
| LSS-Exon1-R | GACACCTGAGGACCACCGGCCAT |
| LSS-Exon2-F | GTGGTCCTAGGTGCTGAGGAGA |
| LSS-Exon2-R | CGTGCTCCTCACGGCTCACCCCT |
| LSS-Exon3-F | CTTGGGCTGTATGTGAAGAGGGT |
| LSS-Exon3-R | CCTAGACCAGGCTGGGCCAGGAT |
| LSS-Exon4-F | GTTGGAGTGAGGTGCTCAGGAGGA |
| LSS-Exon4-R | GCAGCTGCCTGGAAACCCAAGCAT |
| LSS-Exon5-F | GCATTCTTAGTTTTCTGAGGAAACTC |
| LSS-Exon5-R | CCACTGTTTCAGCTGCAAGTGCAT |
| LSS-Exon6-F | CAGAGGGTGAAGCTTCCCAGCT |
| LSS-Exon6-R | GCTGTCACAGCCTGCACCTGAC |
| LSS-Exon7-F | GAAAGGGCCCAAGGTATGGATGCT |
| LSS-Exon7-R | GTGAGTGGACAGGTGTGGTTAGAT |
| LSS-Exon8-F | GAGCCAGGCCTACCAGGTGCT |
| LSS-Exon8-R | GCAGGGGATGAGTGCGTGAAT |
| LSS-Exon9-F | GCAGTGCATGGAGCTCCAGGCT |
| LSS-Exon9-R | CCAGGAAACCCCACTCCCAGCT |
| LSS-Exon10-F | GTGGATCTGGACGAGACCTTGT |
| LSS-Exon10-R | CACTGGGATGCAGCTGGGGCT |
| LSS-Exon11-F | GTGCAGGGTCTGGGTAGCAGCT |
| LSS-Exon11-R | GACATGATTGCAAAGGAAGCAT |
| LSS-Exon12-F | CTGGAGGCAGTGGCTGGGAGT |
| LSS-Exon12-R | GCAAGTGTGTGGCCAGCAGTGCT |
| LSS-Exon13-F | GGCAGGATGTGGCCAGGACCAT |
| LSS-Exon13-R | GCACTTCTGCCTGCAGGAGCT |
| LSS-Exon14-F | CCAGTCTGTCTCAGCGATGT |
| LSS-Exon14-R | CCAAAAACGCCAAGGGAGGAGT |
| LSS-Exon15-F | CTGGCTGCACCCACACCTTTGGT |
| LSS-Exon15-R | GCTCATCTGCAGGACACGAGGT |
| LSS-Exon16-F | GTTGTCAGCCCTAGTGTTGCCT |
| LSS-Exon16-R | CAGGTTTGTGTACCACAGTGCT |
| LSS-Exon17-F | GAGCTGCAGAGCCTGGGCAGCCA |
| LSS-Exon17-R | CCGTGTCACAGAATGATGCGT |
| LSS-Exon18-F | GAATTGGGATAGGTAAACTGCT |
| LSS-Exon18-R | CGCAGTGTGTGAGAGCAGAAACCT |
| LSS-Exon19-F | CTTAATGCCTGAGGCACTGGAGT |
| LSS-Exon19-R | CACTCATGACAGAGCATTGGGTT |
| LSS-Exon20-F | CAAGGCAGCCTGCTGGGGTGA |
| LSS-Exon20-R | CACCGGCTCACAGCTGAGTGT |
| LSS-Exon21-F | CTCACTGCAGCATTCCAGGGTT |
| LSS-Exon21-R | GTGGAAACAGCCATGCACGCT |
| LSS-Exon22-F | GCCAACAGCCAGGGCTCCAGTT |
| LSS-Exon22-R | GGTTGGAGCCCAAGACAGGGT |

**b**

| Gene | Primer (5'-3') |
|---|---|
| *αA*-R116C-For | TTCCCGTGAGTTCCACTGCCGCTACCGCCTGCCGTCGCTGC |
| *αA*-R116C-Rev | CGGCAGGCGGTAGCGGCAGTGGAACTCACGGG |
| *αA*-R116H-For | TTCCCGTGAGTTCCACCACCGCTACCGCCTGCCGTCGCCAC |
| *αA*-R116H-Rev | CGGCAGGCGGTAGCGGTGGTGGAACTCACGGG |
| *αA*-Y118D-For | GAGTTCCACCGCCGCGACCGCCTGCCGTCCAACTTACGAC |
| *αA*-Y118D-Rev | CGTTGGACGGCAGGCGGTCGCGGCGGTGGAACT |
| *αB*-R120G-For | CAGGGAGTTCCACGGGAAATACCGGATAGGGGG |
| *αB*-R120G-Rev | GGATCCGGTATTTCCCGTGGAACTCCCT |
| *βB2*-V187E-For | AGGTGCAGTCCGAGCGCCGTATGTGGAG |
| *βB2*-V187E-Rev | ATACGGCGCTCGGACTGCACCT |
| *βB2*-V187M-For | AGGTGCAGTCCATGCGCCGTATGTGATG |
| *βB2*-V187M-Rev | ATACGGCGCTCGGACTGCACCT |
| *βB2*-R188H-For | TGCAGTCCGTGCACCGTATCCCGCCAC |
| *βB2*-R188H-Rev | GGATACGGTGCACGGACTGCA |
| *γC*-G129C-For | CACGTGCTGGAGTGCTGCTGGGCTGC |
| *γC*-G129C-Rev | CAGCAGCACTCCAGCACGTG |
| *γD*-W43R-For | GTGGACAGCGGCTGCCGGATGCTCTATGAGCTGGCGG |
| *γD*-W43R-Rev | GCTCATAGAGCATCCGGCAGCCGCTGTCCAC |

**a**, Primers used for PCR amplification and sequencing of each exon in the human *LSS* gene. **b**, Primers used in construction of crystallin mutants.